SLAC–PUB–5715
UCSB–HEP–92–01
January 1992
(T/E/I/A)

Physics Possibilities at a Photon Linear Collider*

Douglas L. Borden†, Daniel A. Bauer, David O. Caldwell

Physics Department,
University of California, Santa Barbara, CA 93106

and

Stanford Linear Accelerator Center,
Stanford University, Stanford, CA 94309

Submitted to Physical Review D

* Work supported in part by Department of Energy contract DE–AC–76SF00515 and grant DOE–FG–91ER40618.

† Supported in part by a National Science Foundation Graduate Fellowship.

ABSTRACT

With the convergence of linear collider and laser technology, a new type of facility may soon be made available for research in fundamental particle physics: a Photon Linear Collider where high energy photon beams, produced by the Compton backscattering of laser photons off linac electrons, are brought into collision with electron beams or with other photon beams. Control over both the spectral distribution and mean helicity of the photon beam is possible by changing the polarization states of the linac electron beam and laser. In the resulting $e\gamma$ or $\gamma\gamma$ collisions, such control allows one to vary the $e\gamma$ or $\gamma\gamma$ luminosity distribution as well as to produce selectively one particle type over another. Additionally, high luminosities—potentially higher than in e^+e^- collisions—are possible in such a facility, providing an opportunity for a broad and diverse physics program. In particular, a Photon Linear Collider offers a unique environment for the exploration of the Higgs sector of the Standard Model. Tuned to provide a broad luminosity distribution, a $\gamma\gamma$ collider permits the search for an intermediate mass Higgs boson as a resonance in $\gamma\gamma \rightarrow b\bar{b}$ production. Tuned for a more monochromatic spectrum, a $\gamma\gamma$ collider allows a measurement of the two-photon width of the Higgs, a sensitive probe of physics beyond the Standard Model. Clean channels are made available for the discovery of new particles, such as excited electron states, supersymmetric particles, heavy charged particle pairs, or any particles with appreciable two-photon couplings. Precision electroweak tests also benefit from such a machine. Photons in the initial state allow a test of the three-gauge-boson coupling without the complicating effect of γ-Z interference. Both $e\gamma \rightarrow W\nu$ and $\gamma\gamma \rightarrow WW$ offer information on the W boson complementary to that available from $e^+e^- \rightarrow WW$; $e\gamma \rightarrow eZ$ allows a search for anomalous $\gamma\gamma Z$ and γZZ couplings. Finally, a Photon Linear Collider serves as an excellent laboratory for Quantum Chromodynamics tests. Studies of photon structure functions, jet and hadron production, and $b\bar{b}$ and $t\bar{t}$ resonances are all made available at such a facility. In this paper, we review some of the technical aspects of a Photon Linear Collider and utilize Monte Carlo studies to explore some of the physics which might result from high energy $e\gamma$ and $\gamma\gamma$ collisions.

I. INTRODUCTION

While the idea of producing high energy photon beams by Compton backscattering laser light off a beam of linac electrons is not new [1-8], the recent emergence of viable linear collider technology and the development of high power lasers suggests that the possibility of colliding high energy photon beams may become a reality. Although some exploratory work has already been done [9-25], it behooves us now to examine more closely the physics which could actually be accomplished with a Photon Linear Collider (PLC), a machine capable of colliding a photon beam, derived from the backscattering of laser light off a high energy electron beam, with either an electron beam or another photon beam.

There are three main areas of high energy physics concentration one can foresee for the next decade or two: searches for new particles; precision tests of the Standard Model of electroweak interactions; and continued study of the Standard Model of strong interactions, QCD. Of the new particles presently postulated, those constituting the Higgs sector are currently the most sought-after prizes. Although the Standard Model makes do with just a single neutral Higgs, nothing prohibits more complicated Higgs sectors. As an example, the Minimal Superymmetric extension to the Standard Model (MSSM) results in two neutral scalar Higgs, a neutral pseudoscalar, and two charged Higgs bosons [26,27]. Searches at LEP have found no evidence for the Standard Model Higgs up to 48 GeV, with somewhat lower mass limits on neutral MSSM Higgs [28]. LEP-II should extend these limits up to nearly the mass of the Z^0; progress beyond that will require considerable data from the SSC or LHC and probably also from a new e^+e^- linear collider [29,30]. Finding a single neutral scalar boson at any of these machines will likely not be enough to tell if it is the Standard Model Higgs. It will be necessary to produce or exclude neutral Higgs bosons up to several hundred GeV to tell which Higgs scenario is correct, if any. Of particular difficulty is the detection of a neutral Higgs with intermediate mass, say in the range $80 < M_H < 2M_Z$. The only method proposed at hadron colliders for this is the detection of the two-photon decay. A much cleaner method would be the production of Higgs bosons by two-photon collisions. The Standard Model Higgs coupling is small but results in an observable production cross section; the same is generally true of extended Higgs sectors, and photon-photon reactions give access to all of the neutral Higgs particles, as well as to the charged Higgs via pair production [17,29]. More importantly, the coupling of the Higgs to two photons, shown in Fig. 1, involves loops where any new charged fermions or bosons with couplings to the Higgs must contribute, giving crucial information on the nature of the Higgs itself. A measurement of this process would be quite sensitive to new physics even at higher mass scales [17].

Also of great interest is the possibility that all known particles have supersymmetric partners [26,27]. Since we have not yet observed supersymmetric particles, it is clear the symmetry must be broken; most models predict that this generates superpartner masses of around a few hundred GeV or less [31]. The present superpartner mass limits are still rather low [32], and extension to masses greater than about 100 GeV will require new machines; again there has been considerable study of the prospects [33,34]. For the direct production of exotic particles such as supersymmetric partners, where it will be difficult to recognize the nature of the new particle, the two-photon reaction could provide a very clean environment. It has been recognized for some time that pair production via gauge boson fusion represents one of the best ways to produce and study sleptons and squarks [25,35]. Also, $e\gamma$ collisions may provide a particularly nice way to detect single selectrons produced in association

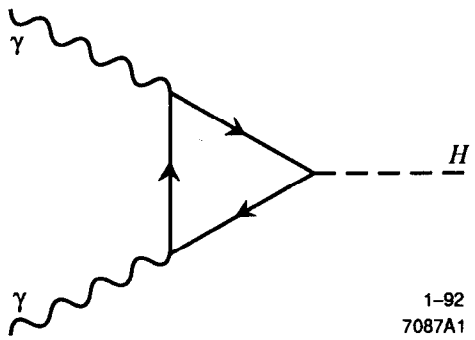

Fig. 1. The coupling of a Higgs to two photons. The coupling proceeds through loops of charged particles which couple to the Higgs. Such a coupling is very sensitive to physics beyond the Standard Model.

with a neutralino [20,23]. Indirect observation of squarks via their effects on the photon structure function may also be possible in $e\gamma$ reactions [24].

Many other possibilities for physics beyond the Standard Model have been proposed which result in new massive particles. There may be another layer of structure within the present 'elementary' particles, resulting in composite quarks and leptons which would manifest themselves as excited states and would have distinctive signatures as they decay into ordinary fermions plus photons [36,37]. Technicolor models assume a composite Higgs boson and predict a number of 'techni-hadrons' above the weak scale [38]. Thus there is a good chance that new particles exist in the mass regime up to 1 TeV, and a multi-pronged approach will yield the best chance of finding, or excluding, them. The $e\gamma$ and $\gamma\gamma$ reactions are generally complementary to the more familiar e^+e^- and hadronic search techniques.

It will continue to be important at future colliders to test the Standard Model of electroweak interactions at higher energies and in as many ways as possible, since it is vital to see where it must yield to a more comprehensive theory. Breakdowns of the theory will surely manifest themselves as non-standard triple-gauge-boson couplings (e.g., $WW\gamma$, WWZ, . . .), even if new particles are not detected [39]. Important Standard Model tests on the nature of vector bosons (e.g., compositeness) should be possible from the study of reactions such as $\gamma\gamma \rightarrow WW$ [10,15,16]. These tests are complementary to, and may be cleaner than, those possible using e^+e^- annihilation, where the analysis is complicated by the presence of WWZ couplings absent in the two-photon reactions. Even better may be a measurement of the process $e\gamma \rightarrow W\nu$ [10-16].

Finally, it will continue to be necessary to probe the theory of strong interactions, QCD, both in the perturbative and non-perturbative regimes. Much remains to be done in the study of hadron spectroscopy and hadro-production: the lowest order quark model nonets have yet to be experimentally completed; little is known about radial excitations; there is a whole spectrum of 'exotic' particles such as four-quark states, $q\bar{q}g$ hybrids, and glueballs which should exist but for which there are presently only hints; and QCD awaits some interesting challenges to its ability to predict the characteristics of hadron production as new kinematic regions are explored [40,41]. The study of two-photon resonance and exclusive hadron production at low energies using virtual bremsstrahlung from storage ring beams has made substantial contributions to our understanding of QCD [42]. The mass reach of this technique, however, is limited. Extending this reach up through the bottomonium, and possibly toponium, sector would result in an enormous improvement in the number of accessible states and in access to kinematic regimes where perturbative QCD predictions should be valid.

In this paper, we explore some of the physics possibilites and technical aspects of producing and colliding photon beams at the next generation of e^+e^- linear colliders, where high energies and very high luminosities are planned. Section II discusses the basic approach to achieve $\gamma\gamma$ and $e\gamma$ collisions, the formalism, and the constraints such reactions would impose on linear colliders and lasers. In Section III, the main physics results that might be achieved at a Photon Linear Collider are discussed. Section IV provides a summary.

II. FORMALISM AND DESIGN ASPECTS OF PHOTON LINEAR COLLIDERS

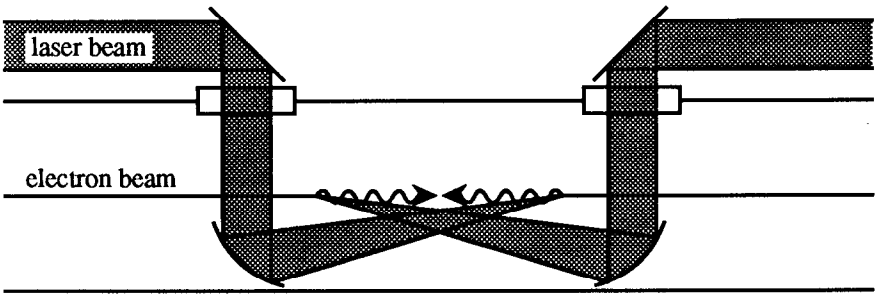

Fig. 2. A schematic design for a Photon Linear Collider. Laser beams are brought into the beampipe and are focused on the electron beams from a linear collider. The laser photons are Compton back-scattered, resulting in intense beams of high energy photons.

A. Basic Idea

We first introduce the basic idea of producing real, high energy photon beams and colliding them with either electron or photon beams. The idea is now rather old and has many variations but all revolve around the collision of a high-power, approximately optical wavelength laser beam with an intense, high-energy electron beam from a linear collider [1-8]; see Fig. 2. Through the process of Compton backscattering, shown in Fig. 3, the result is a high-energy photon beam which closely follows the original trajectory of the electron beam. The original electrons are degraded substantially in energy but also continue approximately on their original paths.

The first linear collider, SLC, has demonstrated the feasibility of the concept of colliding low emittance beams with very small spot sizes [43]. This has spurred the development of a whole new generation of projects, as shown in Table I. Some of these machines are likely to be available after the turn of the century. In parallel, and for many different purposes, lasers are being developed which combine very high intensity with short pulse lengths and reasonable repetition rates [50]. Thus it becomes possible to contemplate the complete conversion of electron bunches in a linear collider into photon bunches of comparable energy.

Table I. Possible design parameters for linear e^+e^- colliders of the future [44–49].

	NLC/TLC	JLC	CLIC	VLEPP	DESY-THD	TESLA
Center of Mass Energy (GeV)	500/1000	500/1000	2000	1000	500	500/1000
Particles per Bunch (10^{10})	1.5	1.0/1.8	0.5	10	1.0	4.2/6
Bunches per Pulse-train	10	10	1	1	172	400/160
Pulse-trains per Second	120/180	150	1700	100	50	20
IP rms Vertical Beam Size (nm)	4/2.5	2.5/2.3	12	10	40	100/60
IP Aspect ratio	80/88	120/160	5	100	8	10
IP rms Bunch Length (μm)	100	100	200	700	500	2000/1000
Luminosity (10^{33} cm^{-2} s^{-1})	2/10	2/6	1	1	1.5	2/5

B. Compton Cross Section and Kinematics

An optical laser beam of frequency ω_o and circular polarization λ_γ is focused on a beam of linac electrons of energy E_b and longitudinal polarization λ_e a few centimeters upstream of the interaction point (IP). The laser light Compton backscatters off the high energy electrons, resulting in a collimated beam of very high energy photons (of order the original e^- beam energy). Both the scattered electrons and the backscattered photons follow the original e^- beam direction within a few μrad and are therefore incident on the interaction point in a tight final focus. The electrons, however, can be deflected away from the interaction point by a transverse magnetic field in order to reduce backgrounds. It is possible, by varying the polarization of the laser photons and linac electrons, and by exploiting the energy dependence of the photon scattering angle, to obtain a fairly monochromatic luminosity distribution in both $e\gamma$ and $\gamma\gamma$ collisions. It is also possible to choose polarization parameters so as to obtain a broad luminosity distribution, allowing for the search for resonances through their $e\gamma$ or $\gamma\gamma$ couplings.

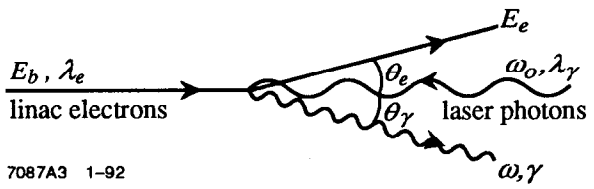

Fig. 3. Compton scattering of an electron of energy E_b and longitudinal polarization λ_e (= ±1) with a laser photon of frequency ω_o ($<<E_b$) and circular polarization λ_γ (= ±1).

The Compton kinematics are characterized by the dimensionless variable

$$x \equiv (4E_b\omega_o/m_e^2)\cos^2(\alpha/2) \approx 15.3\left(\frac{E_b}{\text{TeV}}\right)\left(\frac{\omega_o}{\text{eV}}\right), \tag{2.1}$$

where α is the angle between the electron beam and laser beam, and where we assume $\cos^2(\alpha/2) \approx 1$ (nearly achievable in practice with the use of focusing mirrors to direct the laser beams into the vacuum pipe). The differential Compton cross section (for $\omega \le \omega_{\max} = E_b \frac{x}{x+1}$) is [6]:

$$\frac{1}{\sigma_c}\frac{d\sigma_c}{d\omega} \equiv f(\omega) = \frac{1}{E_b\sigma_c}\frac{2\pi\alpha^2}{xm_e^2}\left[\frac{1}{1-y} + 1 - y - 4r(1-r) - \lambda_e\lambda_\gamma rx(2r-1)(2-y)\right], \tag{2.2}$$

where $y = \omega/E_b$, $r = \frac{y}{x(1-y)} \le 1$, and where the total Compton cross section σ_c is

$$\sigma_c = \sigma_c^0 + \lambda_e\lambda_\gamma\sigma_c^1$$

$$\sigma_c^0 = \frac{\pi\alpha^2}{xm_e^2}\left[\left(2 - \frac{8}{x} - \frac{16}{x^2}\right)\ln(x+1) + 1 + \frac{16}{x} - \frac{1}{(x+1)^2}\right] \tag{2.3}$$

$$\sigma_c^1 = \frac{\pi\alpha^2}{xm_e^2}\left[\left(2 + \frac{4}{x}\right)\ln(x+1) - 5 + \frac{2}{x+1} - \frac{1}{(x+1)^2}\right]$$

The backscattered photon energy distribution is plotted in Fig. 4 for unpolarized beams and for various values of the x parameter. The spectrum becomes harder as x increases. One might be tempted to strive for as high an x value as one could by using the highest frequency laser available, and thereby achieve the hardest photon spectrum possible. Unfortunately, as x is increased processes other than Compton scattering become possible, introducing backgrounds and altering the resulting photon spectrum. The most important of these processes is the conversion of a high energy photon into an e^+e^- pair in a collision with a laser photon farther along in the laser pulse [8]. The threshold $\omega_{max}\omega_o = m_e^2$ for this reaction occurs at $x = 2(1+\sqrt{2}) \approx 4.83$. The result is a depletion of the highest energy photons from the spectrum, as demonstrated in Fig. 5. Not only does pair conversion degrade the photon spectrum, but the resulting e^+e^- pairs represent an additional beam background with which to be concerned. In order to avoid such effects, in this paper we consider only designs with $x < 4.83$.

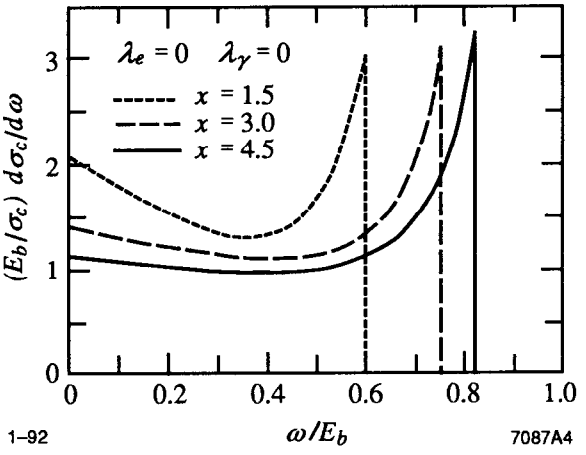

Fig. 4. Energy spectrum of high energy photons from Compton backscattering with unpolarized beams for various x values.

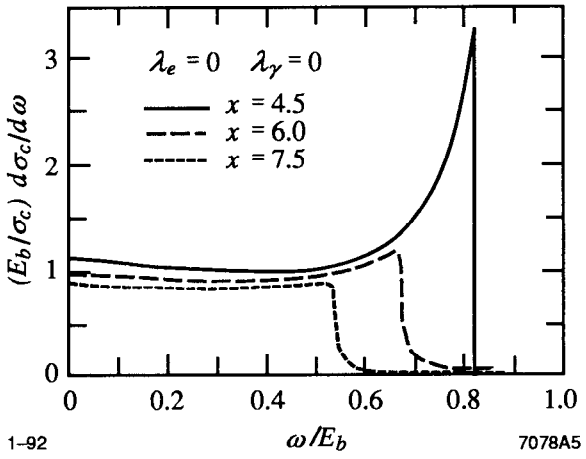

Fig. 5. Backscattered photon spectrum for unpolarized beams at x values below and above threshold for pair conversion of the highest energy photons in the laser pulse. The reconversion of the high energy photons into e^+e^- pairs is exaggerated by assuming a very dense laser photon pulse, which ensures a high probability that a photon reconverts if kinematically allowed.

Polarizing both the electron beam and the laser results in a substantial change in the photon spectrum: if the electrons and laser are like-polarized (both right-handed or both left-handed), then the resulting photon spectrum is relatively flat; if the electrons and laser are oppositely polarized, the resulting spectrum is more monochromatic, peaking at very high energy (Fig. 6). Polarizing the electrons or laser also results in polarized high energy photons. The mean scattered photon helicity depends on the energy of the photon and is given by:

$$\lambda(\omega) = \frac{\lambda_\gamma(1-2r)(1-y+\frac{1}{1-y}) + \lambda_e rx\left[1+(1-y)(1-2r)^2\right]}{1-y+\frac{1}{1-y}-4r(1-r)-\lambda_e\lambda_\gamma rx(2r-1)(2-y)}, \tag{2.4}$$

where y and r are defined as in Eq. 2.2 [6]. Notice that the backscattered photons have non-zero polarization when *either* electrons *or* laser photons are polarized. Figure 6 shows the mean photon helicity in two extreme cases, overlaid with the resulting photon energy spectrum. Note that the flat spectrum (obtained by backscattering electrons and laser photons with the same handedness) has nearly maximum mean photon helicity over almost the whole energy range, whereas the peaked spectrum has opposite helicities for low and high energies.

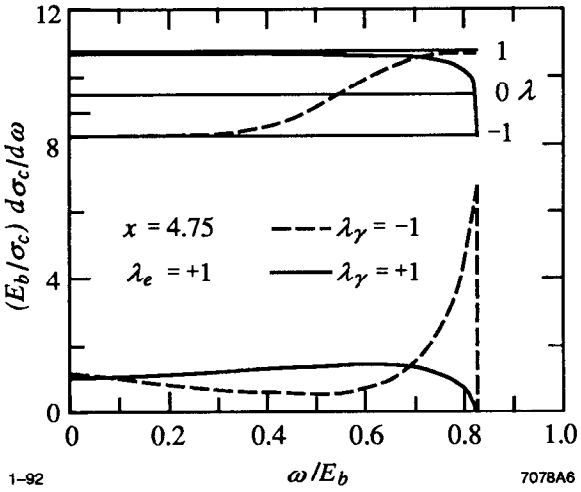

Fig. 6. Helicity and energy spectrum of backscattered photons for Compton scattering with polarized beams.

After Compton scattering, both the electrons and photons travel essentially along the original e^- beam direction. The photon and electron scattering angles are unique functions of the photon or electron energy and (for θ small) are given by

$$\theta_\gamma(\omega) \approx \frac{m_e}{E_b}\sqrt{\frac{E_b x}{\omega} - (x+1)} \tag{2.5}$$

$$\theta_e(E_e) \approx \frac{m_e}{E_b}\sqrt{\frac{E_b}{E_e}\left(2 + x - \frac{E_b}{E_e}\right) - (x+1)}$$

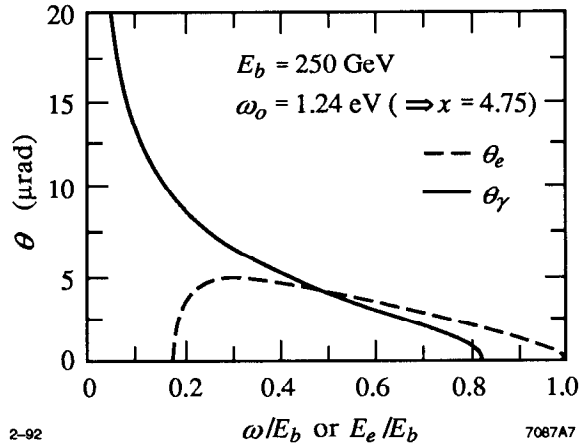

Fig. 7. Electron and photon scattering angles for a typical beam energy and x value. The numerical value of θ scales inversely with E_b but the overall shape depends only on x.

These functions are displayed in Fig. 7 for a typical beam energy of 250 GeV and laser energy of 1.24 eV. The high energy photons scatter at very small angles (a few microradians), while the softest photons scatter the most; the electrons are only slightly deflected from their original direction and scatter into a narrow cone.

C. The $e\gamma$ and $\gamma\gamma$ Luminosity Distributions

The high energy photon beam produced from one beam of a linear collider can be brought into collision with the other electron beam, resulting in $e\gamma$ collisions, or into collision with a similarly produced photon beam from the other electron beam, resulting in $\gamma\gamma$ collisions. Because of the small, but finite, photon scattering angles, the resulting luminosity distributions depend sensitively

on the conversion distance (distance from the conversion point—where the laser pulse intersects the electron beam—to the interaction point) and on the size and shape the electron beam would have had at the interaction point in the absence of a backscattering laser.

Define z as the distance from conversion point to interaction point, and consider an electron on a path which intersects the interaction plane at a point (x_o,y_o); see Fig. 8. A photon scattering off this electron at a polar angle θ and azimuthal angle β intersects the interaction plane at a point (x,y) given by

$$(x,y) = (x_o + z\theta\cos\beta,\ y_o + z\theta\sin\beta). \tag{2.7}$$

If $\rho_e(x,y)$ is the transverse density of the original electron beam at the interaction point, then the density of photons (which scatter at this polar and azimuthal angle) is

$$\rho_\gamma(x,y;\theta,\beta) = \rho_e(x - z\theta\cos\beta,\ y - z\theta\sin\beta). \tag{2.8}$$

If $z\theta$ is much smaller than typical beam spotsize dimensions, the photons arrive at the interaction point in as tight a final focus as the electrons would have. However, if $z\theta$ is much larger than typical beam spotsize dimensions, then the photon interaction point is much larger than the original electron spotsize, resulting in a loss of luminosity. For beam energies of several hundred GeV and conversion distances of a few centimeters, $z\theta$ is of order several tens of nanometers, which is close to the typical spotsize dimensions envisioned for the next generation of linear colliders. Thus, in designing a PLC neither limit will strictly hold, and the luminosity of the PLC will depend sensitively on the particular machine parameters chosen.

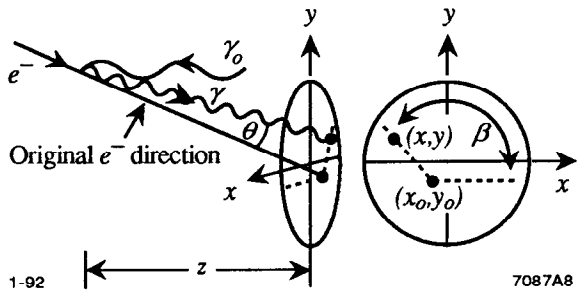

Fig. 8. An electron whose path intersects the interaction plane at (x_O,y_O) encounters a laser photon (γ_O) a distance z prior to the interaction plane. The laser photon backscatters at polar angle θ and azimuthal angle β, intersecting the interaction plane at the point (x,y).

For simplicity consider an electron beam with azimuthal symmetry:

$$\rho_e(x,y) = F_e\left(\sqrt{x^2+y^2}\right) \equiv F_e(r) \tag{2.9}$$

(i.e., $\rho_e(x,y)\,dx\,dy = F_e(r)r\,dr\,d\phi$, where $\phi = \arctan(y/x)$). After Compton backscattering, the probability that a given photon will be found with energy ω intersecting the interaction plane at (r,ϕ) is

$$P_\gamma(r,\phi,\omega)=\frac{f(\omega)}{2\pi}\int_0^{2\pi}d\beta\,F_e\left(\sqrt{r^2+z^2\theta_\gamma(\omega)^2-2rz\theta_\gamma(\omega)\cos\beta}\right). \tag{2.10}$$

As $P_\gamma(r,\phi,\omega)$ doesn't depend on ϕ, we will often use $P_\gamma(r,\omega)\equiv P_\gamma(r,\phi,\omega)$.

Consider the collision of a high energy backscattered photon beam with a linac electron beam. In the interaction plane the probability of finding a given electron with energy E at (r,ϕ) is

$$P_e(r,\phi,E)=\delta(E-E_b)F_e(r). \tag{2.11}$$

The $e\gamma$ differential luminosity is then

$$\frac{dL_{e\gamma}}{d\omega}=2\pi N_1N_2\int_0^\infty r\,dr\,F_{e1}(r)P_{\gamma 2}(r,\omega), \tag{2.12}$$

where the beam moving along the positive (negative) z-axis is indicated with a subscripted 1 (2). In the absence of the backscattering laser, the ee luminosity is

$$L_{ee}=2\pi N_1N_2\int_0^\infty r\,dr\,F_{e1}(r)F_{e2}(r), \tag{2.13}$$

so the normalized differential $e\gamma$ luminosity is

$$\frac{1}{L_{ee}}\frac{dL_{e\gamma}}{d\omega}=\frac{\int_0^\infty r\,dr\,F_{e1}(r)P_{\gamma 2}(r,\omega)}{\int_0^\infty r\,dr\,F_{e1}(r)F_{e2}(r)}. \tag{2.14}$$

Making a change of variable,

$$W=2\sqrt{\omega E_b}=e\gamma \text{ invariant mass}, \tag{2.15}$$

the $e\gamma$ luminosity distribution is

$$\frac{1}{L_{ee}}\frac{dL_{e\gamma}}{dW}=\frac{W}{2E_b}\frac{\int_0^\infty r\,dr\,F_{e1}(r)P_{\gamma 2}(r,\frac{W^2}{4E_b})}{\int_0^\infty r\,dr\,F_{e1}(r)F_{e2}(r)}. \tag{2.16}$$

Now consider the collision of two high energy backscattered photon beams. The $\gamma\gamma$ differential luminosity is

$$\frac{1}{L_{ee}}\frac{dL_{\gamma\gamma}}{d\omega_1\, d\omega_2}=\frac{\int_0^\infty r\,dr\,P_{\gamma 1}(r,\omega_1)P_{\gamma 2}(r,\omega_2)}{\int_0^\infty r\,dr\,F_{e1}(r)F_{e2}(r)}. \tag{2.17}$$

Making the variable changes,

$$W=2\sqrt{\omega_1\omega_2}=\gamma\gamma \text{ invariant mass}$$

$$\eta=\tanh^{-1}\left(\frac{\omega_1-\omega_2}{\omega_1+\omega_2}\right)=\gamma\gamma \text{ rapidity}, \tag{2.18}$$

the $\gamma\gamma$ luminosity distribution is

$$\frac{1}{L_{ee}}\frac{dL_{\gamma\gamma}}{dW\,d\eta}=\frac{W}{2}\frac{\int_0^\infty r\,dr\,P_{\gamma 1}(r,\frac{We^{\eta}}{2})P_{\gamma 2}(r,\frac{We^{-\eta}}{2})}{\int_0^\infty r\,dr\,F_{e1}(r)F_{e2}(r)}. \tag{2.19}$$

For definiteness we take a Gaussian profile for the electron beams and assume azimuthal symmetry. The electron density at the interaction point is

$$F_e(r)=\frac{1}{2\pi\sigma^2}\,e^{-\frac{r^2}{2\sigma^2}}, \tag{2.20}$$

so the corresponding photon density is

$$P_\gamma(r,\phi,\omega)=\frac{f(\omega)}{2\pi\sigma^2}\,I_o\left(\frac{rz\theta_\gamma(\omega)}{\sigma^2}\right)e^{-\frac{r^2+z^2\theta_\gamma(\omega)^2}{2\sigma^2}}, \tag{2.21}$$

where I_o is the modified Bessel function of order 0. The $e\gamma$ luminosity is then

$$\frac{1}{L_{ee}}\frac{dL_{e\gamma}}{dW}=\frac{W}{2E_b}f(\tfrac{W^2}{4E_b})e^{-\frac{d^2}{2(\sigma_1^2+\sigma_2^2)}}, \tag{2.22}$$

where $d\equiv z\theta_\gamma(\frac{W^2}{4E_b})$, and the $\gamma\gamma$ luminosity is

$$\frac{1}{L_{ee}}\frac{dL_{\gamma\gamma}}{dW\,d\eta}=\frac{W}{2}\,f_1(\tfrac{We^{\eta}}{2})f_2(\tfrac{We^{-\eta}}{2})I_o\left(\frac{d_1d_2}{\sigma_1^2+\sigma_2^2}\right)e^{-\frac{d_1^2+d_2^2}{2(\sigma_1^2+\sigma_2^2)}}, \tag{2.23}$$

where $d_1\equiv z_1\theta_{\gamma 1}(\frac{We^{\eta}}{2})$ and $d_2\equiv z_2\theta_{\gamma 2}(\frac{We^{-\eta}}{2})$.

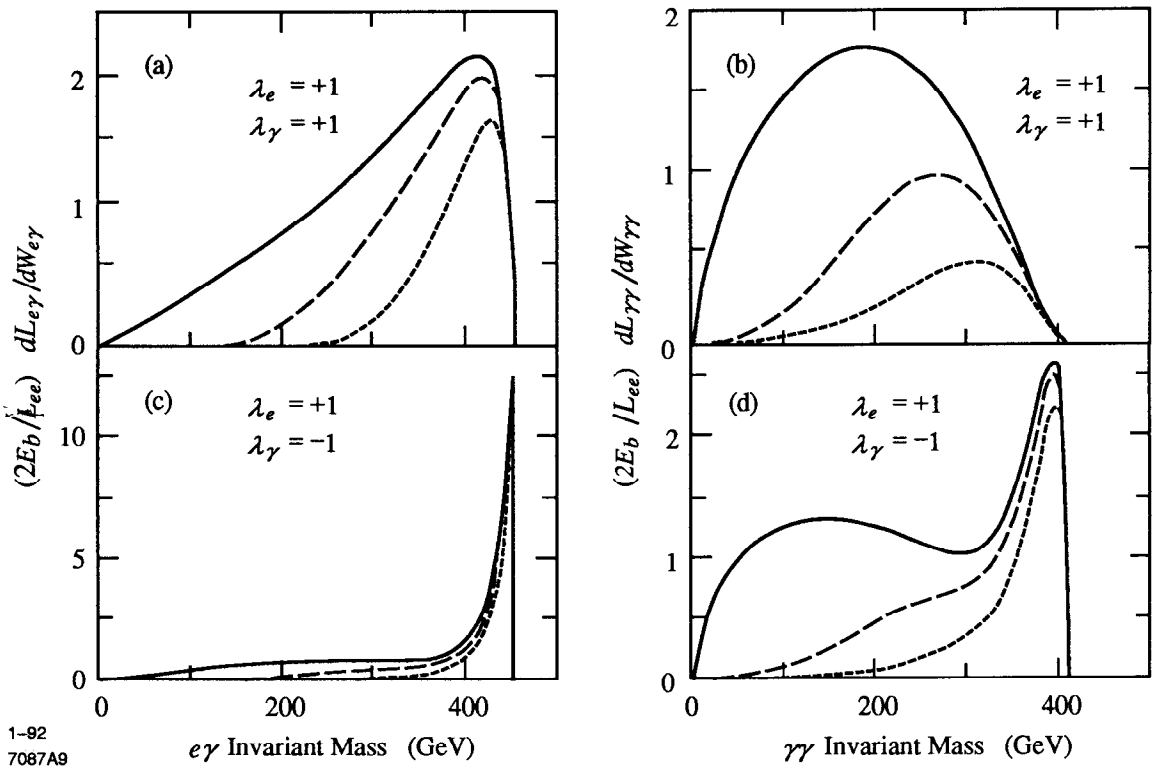

Fig. 9. The $e\gamma$ and $\gamma\gamma$ luminosity distributions for various polarization combinations and for various conversion distances. The vertical axis is dL/dW in units of $L_{ee}/2E_b$. In each figure an electron beam energy of 250 GeV and laser beam frequency of 1.24 eV are assumed. In (a) and (c) one of the electron beams has been converted to photons; in (b) and (d) both electron beams have been converted to photon beams. The electron beam spotsize σ is 100 nm and in each figure three conversion distances are illustrated: $z = 0$ cm (solid); $z = 2.5$ cm (long dashes); and $z = 5.0$ cm (short dashes).

Plotted in Fig. 9 are $e\gamma$ and $\gamma\gamma$ luminosity distributions for various polarization combinations and for various conversion distances at typical values of the machine parameters. For simplicity we have assumed that each electron has scattered once and only once in the laser photon pulse—that is, we have ignored the effects on the luminosity distribution of both unscattered electrons and multiple scattering. In the $\gamma\gamma$ examples the rapidity has been integrated out. The primary effect of increasing the conversion distance is to decrease the luminosity at the low-mass end of the spectrum, as the lowest energy photons scatter far away from the beam line. For most purposes this is a beneficial effect, as a more monochromatic distribution makes for a cleaner initial state.

For resonance search purposes a broad luminosity distribution is desirable, and Fig. 9 seems to indicate that this can be obtained only with a very small conversion distance. This is not necessarily the case, for in Fig. 9 we have made the simplifying assumption that each electron scatters once and only once in the laser photon pulse. For sparse laser pulses (whose column density is $<< 1/\sigma_C$) only a small fraction of the electrons scatter and the total $e\gamma$ or $\gamma\gamma$ luminosity achieved is reduced; the shape of the distribution, however, is as is shown in Fig. 9. For dense

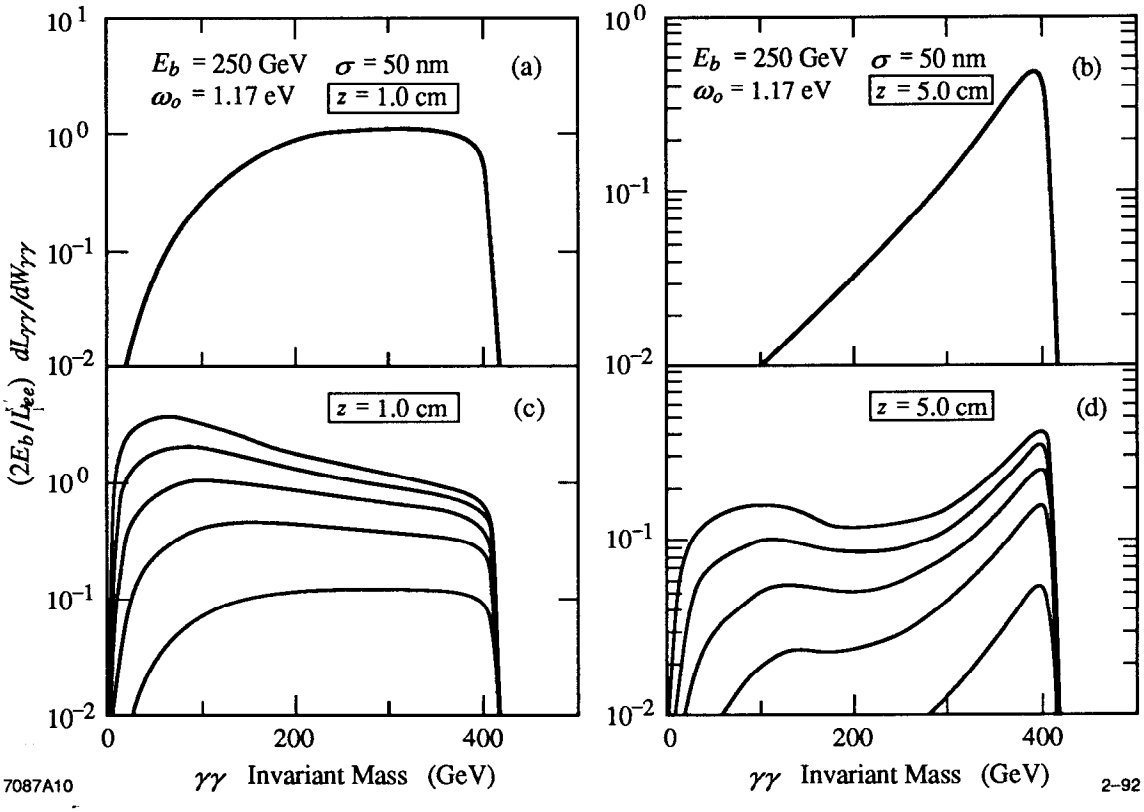

Fig. 10. The $\gamma\gamma$ luminosity distributions resulting from unpolarized Compton scattering in laser pulses of different density at two different conversion distances. (a) and (b) represent the 'ideal' distributions resulting if each electron scatters exactly once in the photon pulse; (c) and (d) represent the more realistic distributions resulting from scattering through different interaction lengths in the laser pulse. The lowest curves in (c) and (d) represent a photon pulse 0.4 interaction lengths long (2×10^{24} γ/cm^2); each successive curve represents an additional 0.4 interaction lengths. At high laser pulse densities (~10^{25} γ/cm^2; the highest curves in (c) and (d)) the luminosity at low invariant mass is dominated by the photons from secondary electron scatters.

laser pulses (with column densities > $1/\sigma_C$) the electron multiple scatters in the laser pulse; in this case photons from secondary electron scatters contribute to the luminosity. In general these secondary photons populate the low energy end of the spectrum, resulting in enhanced $e\gamma$ or $\gamma\gamma$ luminosity at low invariant mass, with little effect on the high-end luminosity.

In Fig. 10 is plotted the $\gamma\gamma$ luminosity distribution resulting from unpolarized Compton backscattering in laser pulses of varying density, as determined from Monte Carlo simulations. The total Compton cross section, σ_C, at these energies is ~2×10^{-25} cm^2. The lowest curve in (c) and (d) corresponds to a laser photon column density of 2×10^{24} cm^{-2} (0.4 interaction lengths), and each successive curve corresponds to an additional 2×10^{24} photons/cm^2. At 10^{25} photons/cm^2 (2.0 interaction lengths, the highest curve in (c) and (d)) the photons from secondary electron scatters have raised the $\gamma\gamma$ luminosity at low invariant mass by several orders of magnitude.

We have assumed round beams in the above examples, but the luminosity spectrum is not strongly dependent on the shape of the beam; it is the size that is most important. The flat,

ribbon-like beams proposed for some e^+e^- colliders (to minimize beamstrahlung) are obviously impractical, as the vertical dimension is much smaller than typical photon transverse scattering distances, resulting in a loss of luminosity. Moderately elliptical beamshapes, however, lead to luminosity distributions similar to those from round beams, as their height and width are of the same scale.

It is useful to compare and contrast the backscattered laser scheme for creating photon beams with the two other methods often discussed: virtual bremsstrahlung [51] and beamstrahlung [52,53]. Virtual bremsstrahlung is the emission of a virtual photon by an electron in a 'grazing' (low-momentum transfer) collision with a positron or another electron. This process has been the source of all two-photon work done at e^+e^- storage rings to the present and has proven to be a successful method for probing the strong scale of the Standard Model (of order 1 GeV) [42]. Unfortunately, the virtual bremsstrahlung photon flux drops dramatically with increasing mass, so that this method will prove intractable for probing the Weak scale. Beamstrahlung is the bremsstrahlung emission of a real photon by an electron (positron) as it traverses the strong electromagnetic field in the opposing positron (electron) bunch in an e^+e^- collider. Beamstrahlung promises to be an important consideration in the design of future e^+e^- linear colliders, where its effects are generally seen to be undesirable as it results in a broadening of the machine energy and limits the maximum luminosity achievable. Beamstrahlung, however, obviously provides a source of photons for $e\gamma$ and $\gamma\gamma$ physics [52,53]. Like virtual bremsstrahlung, its luminosity distribution is peaked at low photon energies, but falls less drastically with rising energy.

Plotted in Fig. 11(a) is a comparison of the photon spectra from the three sources. The Compton spectrum assumes unpolarized beams at an x value of 4.75 with no multiple scattering and conversion at the IP; the beamstrahlung spectrum results from bunch parameters chosen to maximize the photon yield, with 10^{10} particles ($e^{\pm}$) in a uniform cylindrical bunch of radius 35 nm

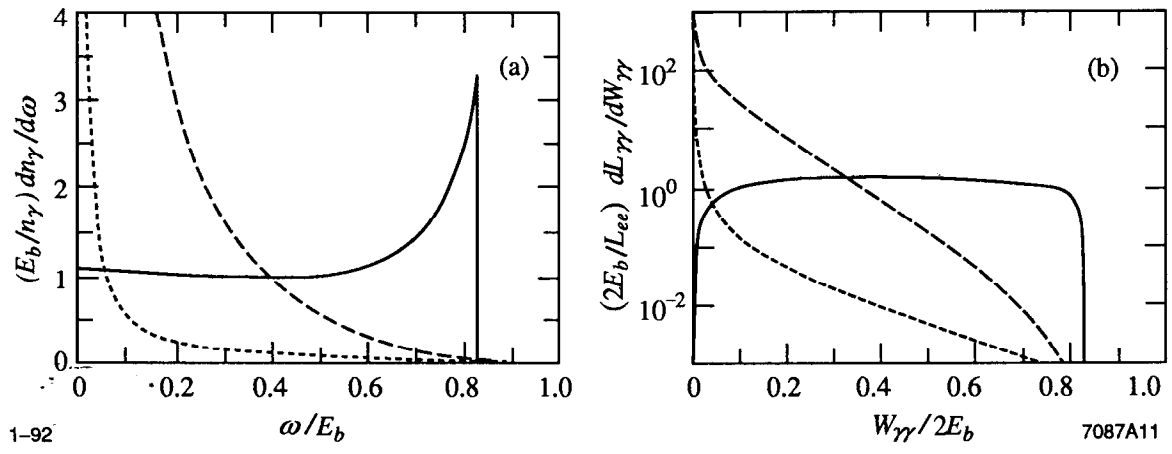

Fig. 11. A comparison of (a) photon energy distributions and (b) $\gamma\gamma$ luminosity distributions for virtual bremsstrahlung (short dashes), beamstrahlung (long dashes), and backscattered lasers (solid).

and length 300 μm (corresponding to a C value of 0.5 and y value of 800 in the notation of Blankenbecler and Drell [52]). Plotted in Fig. 11(b) are the resulting $\gamma\gamma$ luminosity distributions. While bremsstrahlung and beamstrahlung photons may play a role for low mass studies, the advantages of laser backscattering for high energies are obvious.

D. The Conversion Region

For a cylindrical electron beam with a Gaussian profile, the transverse density distribution of the beam a distance z before the interaction point is given by

$$F_e(r) = \frac{1}{2\pi\sigma_e(z)^2} e^{-\frac{r^2}{2\sigma_e(z)^2}}, \tag{2.24}$$

where $\sigma_e(z) = \sigma_e^o\sqrt{1+\left(z^2/\beta_e^2\right)}$, σ_e^o is $\sigma_e(z = 0)$, $\beta_e = (\sigma_e^o)^2/\varepsilon$, and ε is the beam emittance. Typical interaction point β functions envisioned for linear colliders are of order a millimeter, so the beam converges linearly on the interaction point over most of its travel from the final focus quadrupole magnets, leveling out to its final size within a few millimeters of the interaction point. In a PLC, the beam passes through a laser pulse a few centimeters upstream of the interaction point. In order to achieve an appreciable probability for electron Compton scattering, a number of criteria must be satisfied: the transverse density of laser photons must be of order $(1/\sigma_c)$, and that density must be maintained during the whole time the electron bunch passes through the laser pulse; the electromagnetic field in the laser pulse must be kept low enough that each electron interacts with only one laser photon rather than coherently with the total electromagnetic wave; and the electron beam cross section must be at least as small as that of the laser pulse when the two intersect.

The Compton cross section, σ_c, is of order 2×10^{-25} cm^2, so transverse photon densities near 10^{25} cm^{-2} are required. If a laser of frequency ω_o (or wavelength λ_o) and energy/pulse E is focused to an area A, the transverse photon density n achieved is

$$\begin{aligned}\frac{n}{10^{25}\,\mathrm{cm}^{-2}} &\approx 62.4\left(\frac{E}{\mathrm{Joules}}\right)\left(\frac{\omega_o}{\mathrm{eV}}\right)^{-1}\left(\frac{A}{\mu\mathrm{m}^2}\right)^{-1} \\ &\approx 50.3\left(\frac{E}{\mathrm{Joules}}\right)\left(\frac{\lambda_o}{\mu\mathrm{m}}\right)\left(\frac{A}{\mu\mathrm{m}^2}\right)^{-1}.\end{aligned} \tag{2.25}$$

A laser cannot be focused to an arbitrarily small spotsize, though, to achieve very high densities. Ultimately, diffraction limits the area to which the laser can be focused. The focusing of

Gaussian laser beams follows a relation similar to that given for electrons in Eq. 2.24. A distance d from the point of maximal focus the transverse density distribution of the laser beam is given by

$$F_\gamma(r) = \frac{1}{2\pi\sigma_\gamma(d)^2} e^{-\frac{r^2}{2\sigma_\gamma(d)^2}}, \tag{2.26}$$

where $\sigma_\gamma(d) = \sigma_\gamma^o\sqrt{1+\left(d^2/\beta_\gamma^2\right)}$ and where in the diffraction limit $\beta_\gamma = 4\pi(\sigma_\gamma^o)^2/\lambda_o$ for a laser of wavelength λ_o [8]. Writing the area of the laser beam at maximal focusing as $A = \pi(\sqrt{2}\sigma_\gamma^o)^2$ we see that $A = \beta_\gamma\lambda_o/2$. As the laser must remain near maximal focus over the time of passage of the electron pulse, the minimum value of β_γ will be $(l_\gamma + l_e)/2$, where l_γ and l_e are the laser and electron bunch lengths, respectively. This implies a minimum laser beam cross section of $(l_\gamma + l_e)\lambda_o/4$, which leads to a maximum value for the transverse photon density in the laser pulse of

$$\frac{n_{\max}}{10^{25}\,\mathrm{cm}^{-2}} \approx 0.20\left(\frac{E}{\mathrm{Joules}}\right)\left(\frac{l_\gamma + l_e}{\mathrm{mm}}\right)^{-1}. \tag{2.27}$$

It is reasonable to expect lasers will be available with pulse energies near 10 Joules; for such lasers and for electron and laser pulses of length 200 μm, densities near 5×10^{25} cm^{-2} are achievable. Note that for laser wavelengths near 1 μm and these bunch lengths, the laser spotsize is near 100 μm^2.

In a very intense laser pulse, the electromagnetic fields can be very high, leading to multiphoton (coherent) processes such as $e + n\gamma_o \rightarrow e\gamma$ and $\gamma + n\gamma_o \rightarrow e^+e^-$ (where e and γ represent high energy electrons and photons respectively, and γ_o denotes a laser photon). In general, such multiphoton processes will be undesirable in a PLC, as they tend to soften the spectrum and lead to higher backgrounds (e^+e^- pairs) [54]. The importance of multiphoton processes is characterized by the dimensionless parameter ξ, given by

$$\xi^2 = \frac{E}{V}\frac{4\pi\alpha}{m_e^2\omega_o^2}, \tag{2.28}$$

where E is the laser pulse energy, V the pulse volume, and ω_o the laser frequency [54]. At $\xi^2 << 1$ coherent processes are negligible compared with single laser-photon processes; at $\xi^2 >> 1$ multiphoton processes dominate [8,54]. Given a laser of wavelength λ_o, energy/pulse E, and pulse length l_γ, focused to an area A, ξ^2 is given by

$$\xi^2 \approx 11.0\left(\frac{E}{\mathrm{Joules}}\right)\left(\frac{\lambda_o}{\mu\mathrm{m}}\right)^2\left(\frac{l_\gamma}{\mathrm{mm}}\right)^{-1}\left(\frac{A}{\mu\mathrm{m}^2}\right)^{-1}. \tag{2.29}$$

We see that for a 10 Joule laser with wavelength of 1 μm and pulse-length of 200 μm, focused to an area of 100 μm^2, $\xi^2 = 5.5$, well into the multiphoton regime. If the laser pulse-length is lengthened to 2 mm, so the diffraction limited area is 550 μm^2 (assuming an electron pulse-length of 200 μm), then $\xi^2 = 0.1$ and multiphoton processes cease to be important. Note that in this latter case, the maximum photon column density achievable (given by Eq. 2.27) is 9×10^{24} γ/cm^2.

It is interesting to note the relation between ξ^2 and the laser column density. Writing $n_o \equiv 1/\sigma_c \approx 5\times10^{24}$ cm^{-2}, we find

$$\xi^2 \approx 0.11\left(\frac{\lambda_o}{\mu m}\right)\left(\frac{l_\gamma}{mm}\right)^{-1}\frac{n}{n_o}. \tag{2.30}$$

For $n/n_o \approx 1$, long laser pulses (~1 mm or ~3 ps) will be required to suppress coherent interactions in the conversion region.

In order for the electron bunch to convert fully to high energy photons, the electron beam must intercept the laser pulse when the electron beam's transverse size is less than that of the laser pulse; this determines the maximum allowable conversion distance. For $z >> \beta_e$, $\sigma_e(z)$ is given by $\sigma_e(z) = \sigma_e^o z/\beta_e$. Setting $\sigma_e(z_{max}) = \sqrt{A/(2\pi)}$ (where A is the laser pulse transverse area), gives

$$\frac{z_{max}}{cm} \approx 40\left(\frac{\beta_e}{mm}\right)\left(\frac{A}{\mu m^2}\right)^{\frac{1}{2}}\left(\frac{\sigma_e^o}{nm}\right)^{-1}. \tag{2.31}$$

Given an electron beam with a σ_e^o of 50 nm and β function of 2 mm and a laser pulse focused to an area of 100 μm^2, the electron beam must intercept the laser pulse closer than 16 cm from the interaction point. Recalling that the range over which conversion distances should vary (to enable significant control over the luminosity distribution) runs up to only a few centimeters (see Fig. 9), we see that the above limit on the conversion distance is not seriously confining.

E. Linear Collider Parameters for a PLC

In an e^+e^- collider the luminosity per beam crossing is ultimately limited by beam-beam effects. As one bunch passes through the other, the particles emit synchrotron radiation (beamstrahlung) and the bunch shapes are also distorted (disruption). Beamstrahlung broadens the energy spectrum of the electron beams and introduces unwanted backgrounds. Minimizing beamstrahlung tends to increase disruption, eventually 'blowing-up' the beams before they have fully passed through each other. The combined effects of beamstrahlung and disruption set a limit on the maximum achievable luminosity per crossing in e^+e^- collisions [55]. Beam-beam effects, though not absent from a PLC, are much less important [8,56]. For $\gamma\gamma$ collisions, the main constraint is the need to limit coherent pair creation by a photon in the electromagnetic field of the

opposing *electron* beam (the beam used to convert the opposing photon beam). This effect is minimized if the electrons are deflected away from the interaction point after Compton scattering. The situation is slightly more serious in $e\gamma$ collisions: coherent pair creation by the high energy photons in the field of the opposing electron beam joins beamstrahlung and disruption of the colliding e^- beam in the field of the converting e^- beam. Again, if the 'used' converting electrons can be removed from the interaction point, the most serious effects disappear, and only the effect of coherent pair creation remains important. Telnov and Chen have derived limits on the $e\gamma$ and $\gamma\gamma$ luminosity achievable with the constraints of coherent pair creation; these limits are generally much less severe than the corresponding limits placed on e^+e^- colliders [8,56]. Therefore, the total luminosity attainable by a PLC can be greater than that of a comparable e^+e^- machine. Additionally, as positrons are not needed in a PLC, no resources need be devoted to positron generation or regeneration. Eliminating positrons also avoids backgrounds from residual e^+e^- interactions near the photon-photon collision point. Obviously, freed from the constraints of beam-beam effects, it is paramount to try to attain the highest beam currents possible.

It will still be desirable for the linear collider to achieve small beam sizes at a PLC. However, no gain in luminosity is achieved by squeezing the electron beam to smaller dimensions than those dictated by the expected size of the Compton-scattered photon beam at the interaction point. The beam focusing may be simpler for a PLC than for an e^+e^- linear collider if the Compton scattering angles limit one to beam sizes of order 50 nm. In any case, the extremely flat beams needed to minimize beamstrahlung in e^+e^- colliders are not required for a PLC. The beam aspect ratio will be determined more by the needs of the accelerator than the final focus. However, the interaction region will be considerably more complicated due to the need to couple the laser light into the beampipe very close to the collision point and at very small angles relative to the electron beam.

The use of polarized electron beams in a PLC will certainly increase its power as a physics tool, allowing greater control over the luminosity distribution and providing the capability of colliding highly polarized photon beams. Presently, electrons with up to 50% polarization are obtainable at high yield (16 A in a 2.5 nsec pulse) with bulk GaAs sources [57]. Higher polarizations—as high as 86% [58]—have been achieved using strained GaAs lattices and AlGaAs-GaAs superlattices, but not yet at the yields necessary for operation in a high luminosity collider [57,58]. Work in this area is ongoing, however, and there is no reason to doubt that highly polarized electron beams will be available for use in linear colliders.

As will be seen in the next section, one of the most important physics results to be expected from a PLC, the possible discovery and then study of an intermediate mass Higgs boson, favors the use of a moderate energy collider, in the 300–500 GeV range. This would lead to many design simplifications and probably substantial reductions in time and cost. In particular, the choice of RF may be directed towards the well-understood S–band technology instead of the X–band, which is

still under development. The S–band accelerating structures are also more amenable to high beam currents and larger beam spot sizes which are favored for a PLC. The PLC could then also be another, shorter, step on the way to TeV linear colliders with their rich physics program. Alternatively, if cost-effective superconducting accelerating structures can be developed, the very high beam currents achievable in such machines could lead to extremely high $\gamma\gamma$ luminosities, perhaps an order of magnitude higher than in e^+e^- machines.

F. Lasers for a PLC

High power (~10 J), short pulse-length (~1 ps), fast repetition rate (~100 Hz), near visible wavelength (~1 μm) lasers with diffraction-limited beams do not exist yet, but prospects are good that they can be developed well before a PLC can be built [50]. Most linear collider designs achieve luminosity by having many bunches, and each bunch must be of short extent. To deliver all of the photons within the duration of the electron bunch requires a laser pulse length of order a few picoseconds. Ultrashort pulse lasers, formerly of the dye or excimer types, have now been supplanted by solid-state systems, such as titanium-doped sapphire or neodynium-glass. An example of the latter is one which provides more than 10 J in a 0.8 ps pulse by using chirped pulse amplification. This laser gives a focused intensity of more than 4×10^{25} photons/cm^2 from a near diffraction-limited beam of 1.17 eV photons, and hence has all of the desired characteristics except repetition rate [50].

A Lawrence Livermore National Laboratory group has proposed building a Cr:$LiCaAlF_6$ / Cr:$LiSrAlF_6$ laser to use in a test at Stanford Linear Accelerator Center's Final Focus Test Beam Facility [50]. The project would validate the feasibility of Compton-converting linear collider type electron beams to real photon beams and also test the concept of using laser light to collimate the electron beams by scattering away the off-axis beam tails. Although these laser materials would give lower power (~0.1 J into a 10 μm spot) initially, they can be run at much higher repetition rates than a Nd:Glass laser, and the proposers believe that significant increases in both power and repetition rate are possible, so that all of the requirements can be met in the future for a 1.3–1.7 eV laser. Other lasing materials may allow expansion of this range down to ~1 eV, and frequency doubling of such lasers is possible, with only of order a factor of two loss in intensity, enabling an expansion of the frequency range up to as high as ~3.4 eV [59]. This range of frequencies is optimal for use with electron beams of energy from about 100 GeV to about 300 GeV. Converting higher energy beams will require further development of infrared lasers with frequencies below ~1 eV.

However, lasers are not likely to achieve the kHz repetition rate needed to deal with the multi-bunch structure planned for most linear colliders. Instead an optical resonator can be used so that one laser pulse can intersect each of the electron bunches in the pulse-train [50]. The required

photon density (~10^{25} photons/cm^2) needed to convert fully electrons to photons implies ~10^{15} photons in a (100 nm)^2 spot, whereas there are only 10^{10} electrons per bunch. Thus, each bunch encounter with the photon pulse as it bounces within the resonator cell depletes a negligible number of photons, and the laser need only fire at the rate of bunch trains (~100 Hz). While present high power lasers are still about an order of magnitude away from this, the goal seems achievable within a few years.

G. Detector Considerations

To give some reality to our Monte Carlo physics studies, described in the next section, we have chosen to simulate our physics processes using the SLD, the only detector at an operating linear collider, the SLC [43]. Table II lists some of the important specifications of the SLD [60]. While an excellent detector for the Z° physics for which it was designed, the SLD is not optimized for the reactions or the energies considered here. Thus, although our simulations yield promising event rates, it is likely that they would be considerably higher with an optimized detector. Particular weaknesses of the SLD for our uses are inadequate angular coverage of the vertex detector, insufficient magnetic field for good momentum resolution at high energy, insufficiently fine segmentation and depth of the calorimetry, and a general lack of low polar angle detectors. A larger, more hermetic detector would of course be desirable.

One unusual requirement on the detector at a PLC might be the necessity of having a magnetic field transverse to the beam direction at the interaction point. Following Compton scattering, such

Table II. Important SLD specifications.

Tracking	Drift Chamber
Magnetic Field	0.6 T
Momentum Resolution ($\delta p/p$)	0.0015 (p/GeV) (high p)
Two-Track Separation	1.0 mm
Electromagnetic Calorimetry	Lead / Liquid Argon
Depth	22 radiation lengths
Energy Resolution ($\delta E/E$)	$8\%/\sqrt{E/GeV}$
Segmentation	33 mrad × 36 mrad
Angular Resolution	5 mrad
Hadronic Calorimetry	Lead / Liquid Argon + Iron / Gas
Depth	7 interaction lengths
Energy Resolution ($\delta E/E$)	$55\%/\sqrt{E/GeV}$
Segmentation	66 mrad × 72 mrad
Angular Resolution	10 mrad
Vertexing	Silicon CCD Pixel Device
Particle Identification	Cerenkov Ring Imaging Device

a field would bend the electrons away from the collision point to minimize backgrounds. The field required to bend electrons of momentum p a distance δ, given a conversion distance z, is

$$\frac{B}{\text{Tesla}} = 0.067\left(\frac{p}{\text{GeV}}\right)\left(\frac{\delta}{\mu\text{m}}\right)\left(\frac{z}{\text{cm}}\right)^{-2}. \tag{2.31}$$

At a conversion distance of 2 cm, a 250 GeV electron can be deflected 0.5 μm by a 2.1 T magnetic field. Such a field might be generated by superconducting Helmholtz coils placed just outside the beampipe (perhaps between the first and second layers of the vertex detector). Alternatively, if an extremely dense laser pulse is generated, so that each electron undergoes multiple collisions and is degraded in energy to perhaps 25 GeV, then only a 0.2 T field is required. Such a field could be produced by tilting the detector solenoid a few degrees with respect to the collision axis, precluding the need for Helmholtz coils near the interaction point. Obviously, all these considerations will further complicate the already difficult task of engineering the interaction region and beam dump.

III. PHYSICS AT A PLC

A machine capable of colliding photons offers a unique environment in which to pursue particle physics research, an environment orthogonal and complementary to that of the more conventional e^+e^- and hadron colliders. The multitude of physics topics suited for study at a PLC can be divided into four categories. The first consists of those processes involved in the exploration of the spontaneous symmetry breaking sector of the Standard Model, an exploration for which a PLC offers unique opportunities for the possible discovery, but certainly the study, of an intermediate mass neutral Higgs boson. The second class consists of searches for particles outside the Standard Model, including excited states of the electron, supersymmetric particles, and particles with an appreciable coupling to two photons; the unique properties of a PLC allow for particularly clean methods of conducting these searches. We concentrate our effort on these first two classes, using a full Monte Carlo simulation of the physics and, in most cases, a full detector simulation to study these processes in depth. For each process, we simulate a realistic experiment at a PLC. We consider both the physics under investigation (the 'signal') and the primary relevant Standard Model backgrounds. The differential luminosity of the PLC is folded in with the lowest order cross section calculations in a Monte Carlo event generator. The generated events are processed through the Fast Monte Carlo simulation of the SLD Detector [60] at SLAC to simulate a true experimental environment. The resulting 'raw data' is then analysed to try to discern a signal above the background. Such an analysis should provide a fairly realistic, though conservative, assessment of the physics capabilities of a PLC (as SLD is not optimized for the high energies we consider).

The third class of physics consists of precision electroweak studies, in which a PLC may provide a more straightforward determination of properties of the Weak gauge bosons, such as the $WW\gamma$ coupling, than those possible from e^+e^- and pp machines. For this class our analysis is primarily qualitative; no Monte Carlo simulations are utilized. We instead discuss what contribution a PLC may make, concentrating on its sensitivity to different non-standard physics as compared with its e^+e^- and hadron counterparts.

The fourth class consists of studies of strong interactions. Large hadro-production cross sections and a clean initial state available with a PLC make such a machine an excellent laboratory for QCD studies. Again with this class of physics our analysis is primarily qualitative. We list a representative sample of strong interaction physics pursuable at a PLC and discuss the important differences between these processes and the corresponding processes at e^+e^- and hadron colliders.

It will be worthwhile to define some terms and establish some conventions. For a given $e\gamma$ or $\gamma\gamma$ process, it is often most instructive to think in terms of an effective ee cross-section. For an $e\gamma$ or $\gamma\gamma$ machine, the number of events of type X is given by

$$N_X = \int \frac{dL}{dW}\sigma_X(W)dW = L_{ee}\int\left(\frac{1}{L_{ee}}\frac{dL}{dW}\right)\sigma_X(W)dW, \tag{3.1}$$

where L is the $e\gamma$ or $\gamma\gamma$ luminosity and W the $e\gamma$ or $\gamma\gamma$ invariant mass. We then define the effective ee cross-section as

$$\sigma_X^{ee} \equiv \int\left(\frac{1}{L_{ee}}\frac{dL}{dW}\right)\sigma_X(W)dW, \tag{3.2}$$

so that $N_X = L_{ee}\sigma_X^{ee}$. When we quote integrated luminosities, then, we mean the equivalent ee luminosity—the luminosity which would have been attained in the absence of backscattering lasers and neglecting beam-beam effects. This ensures a uniform way to compare the performance of PLC's with vastly different machine parameters: if the underlying electron collider was designed to deliver a luminosity of 10^{33} cm^{-2} sec^{-1}, then all PLC's based on this electron collider will deliver 10^{33} cm^{-2} sec^{-1} of equivalent ee luminosity.

In our Monte Carlo studies of physics at a PLC we have used the 'ideal' $e\gamma$ and $\gamma\gamma$ luminosity distributions of Fig. 9 (which assume each electron scatters exactly once in the laser pulse), rather than the more realistic distributions of Fig. 10 (which correctly account for the probabilistic nature of the Compton scattering). This choice was made principally because including polarization effects in the realistic distributions is difficult, as doing so requires knowledge of the polarization state of an electron following Compton scattering (so that its polarization state would be known for secondary scatters in the laser pulse). Additionally,

calculation of the luminosity distributions in Fig. 10 requires a considerable amount of computer time, and so does not lend itself easily to physics studies in which it is desirable to explore a large volume of PLC parameter space.

Fortunately, the use of the ideal distributions seems justified for the physics studies we consider. It is likely that the use of dense laser pulses—leading to multiple electron scatters, the primary source of the difference between the ideal and actual luminosity distributions—would degrade the high degree of photon polarization attainable assuming only single electron scatters. As will be demonstrated, high photon polarization is a powerful tool for physics at a PLC, so we assume that for most physics purposes a rather sparse laser pulse will be used (perhaps one-half to one interaction length long). Consider a laser pulse 0.7 interaction lengths long. In such a pulse, 50% of the electrons convert, and only 30% of *those* undergo an additional scatter, so in this case the ideal distributions describe the shape of the actual distributions quite well, but lead to an overestimation of the $e\gamma$ luminosity by a factor of two and the $\gamma\gamma$ luminosity by a factor of four. In our studies, rather than rescaling the luminosity distributions to account for unscattered electrons, we compensate for the overestimation of the normalization of the distributions by assuming very conservative values for the total luminosity. Recall that most e^+e^- linear colliders are being designed initially to provide luminosities of (1-2)$\times 10^{33}$ cm^{-2} s^{-1}, but that luminosities at a PLC can be significantly higher due to the absence, or reduced importance, of beam-beam interactions. Thus, we conservatively assume in all of our studies an ee luminosity of only 10^{33} cm^{-2} s^{-1}. This is equivalent, for example, to using a more realistic distribution arising from a laser pulse 0.7 interaction lengths long and assuming an ee luminosity of 2×10^{33} cm^{-2} s^{-1} for an $e\gamma$ collider and an ee luminosity of 4×10^{33} cm^{-2} s^{-1} for a $\gamma\gamma$ collider.

It will be convenient to normalize certain energies to the total energy of the underlying ee machine; as such we define $E_{ee} \equiv 2\sqrt{E_{b1}E_{b2}} = \sqrt{s}$ of the underlying ee machine. When the two electron beams are of equal energy (as will often be the case with $\gamma\gamma$ collisions) we may substitute $2E_b$ for E_{ee}.

A. $\gamma\gamma \rightarrow$ Higgs

The exploration of the spontaneous symmetry breaking sector of the Standard Model promises to occupy much of experimental particle physics over the coming decades. A Photon Linear Collider offers a unique opportunity to search for and study Higgs bosons, and offers its greatest advantage in that energy regime which is least accessible to e^+e^- and hadron colliders.

1. $\gamma\gamma \rightarrow$ Higgs: Discovery

We concentrate on a Higgs boson in the intermediate mass region of 80-180 GeV. A Standard Model Higgs boson below ~48 GeV has already been ruled out by LEP [28], and a Higgs with a

mass between 48 and 80 GeV will either be ruled out or found at LEP-II [29]. For Higgs masses above twice the Z mass, almost certain detection is assured at the SSC or LHC in the 'goldplated' decay mode $H \rightarrow ZZ \rightarrow 4$ leptons [29]. It is the intermediate mass region—from 80 to 180 GeV—which is the most difficult region to access experimentally.

Discovery of an intermediate mass Higgs boson at a hadron collider will most probably occur through the decay of the Higgs to two photons [29]. This $\gamma\gamma$ discovery channel seems tenable for Higgs masses above ~120 GeV, but studies indicate that only a detector with superb electromagnetic calorimetry and photon angle resolution will be capable of extending the range any further down in mass. Associated W production of the Higgs (resulting in the decay mode $WH \rightarrow l\nu\gamma\gamma$) allows for significant background suppression, extending the accessible range all the way down to 80 GeV, but suffers from a very low rate [61,62].

Production of an intermediate mass Higgs boson at an e^+e^- collider proceeds through either the Bjorken process ($e^+e^- \rightarrow ZH$), or through WW fusion ($e^+e^- \rightarrow \nu\bar{\nu}H$). At center-of-mass energies below about 500 GeV the Bjorken process dominates, while above that the WW fusion process is most important [29]. The absence of an energy constraint in WW fusion limits the Higgs mass discovery region accessible at high energy (> 500 GeV) linear colliders to greater than about 130 GeV. At lower $\sqrt{s}$ machines the discovery potential is better, and the mass region accessible extends all the way down to LEP-II limits, but a Higgs boson in the W or Z mass region poses special problems [29,63].

In addition to being the most difficult to access experimentally, the intermediate mass region is also a particularly intriguing region from a theoretical perspective. Weak scale supersymmetry, one of the most compelling solutions to the hierarchy problem and one of the most attractive extensions to the Standard Model, predicts the presence of a Higgs boson near this region. At tree level the theory predicts a Higgs boson with a mass below that of the Z, but radiative corrections push this upper limit well into the intermediate mass region [64-66]. If a Higgs is not found at LEP-II, the presence of a Higgs boson in the intermediate mass region would be a crucial test of Weak Scale supersymmetry.

A $\gamma\gamma$ collider provides an attractive alternative to e^+e^- and hadron colliders for discovering an intermediate mass Higgs boson. The broad luminosity distribution available at a PLC allows a search for a Higgs boson as a resonance in $\gamma\gamma$ collisions. Initially we assume a Standard Model Higgs boson. In the intermediate mass region the Higgs has a very narrow total width (of order a few MeV) and decays predominantly to $b\bar{b}$ [29], so we expect to observe the Higgs as a resonance in $\gamma\gamma \rightarrow b\bar{b}$ production. Because the Higgs is such a narrow resonance, we may safely ignore interference effects between the (u and t channel) continuum diagrams and the (s channel) resonance diagram, so that the $\gamma\gamma \rightarrow b\bar{b}$ cross section decomposes into a sum of a $b\bar{b}$ continuum production cross section and a Higgs Breit-Wigner:

$$\sigma(\gamma\gamma \to b\bar{b}) = \sigma_c(\gamma\gamma \to b\bar{b}) + \sigma(\gamma\gamma \to H \to b\bar{b}) \tag{3.3}$$

$$\frac{d\sigma_c(\gamma\gamma \to b\bar{b})}{d\cos\theta} = \frac{2\pi\alpha^2}{27W^2}\beta\frac{[2-2\beta^4-(1-\lambda_1\lambda_2)(1+\beta^2\cos^2\theta)(1-2\beta^2+\beta^2\cos^2\theta)]}{(1-\beta^2\cos^2\theta)^2} \tag{3.4}$$

$$\sigma(\gamma\gamma \to H \to b\bar{b}) = \frac{8\pi\Gamma(H \to \gamma\gamma)\Gamma(H \to b\bar{b})}{(W^2-M^2)^2+\Gamma_T^2M^2}(1+\lambda_1\lambda_2), \tag{3.5}$$

where $\beta = \sqrt{1-\left(4m_b^2/W^2\right)}$ [18,67]. The Higgs-γ-γ coupling proceeds through loops of charged particles (Fig. 1). In the Standard Model, the $\gamma\gamma$ width is given by [29]

$$\Gamma(H \to \gamma\gamma) = \frac{\alpha^2}{256\pi^3}\frac{M^3}{v^2}\left|\sum_i N_{ci}q_i^2F_i\left(\frac{4m_i^2}{M^2}\right)\right|^2, \tag{3.6}$$

where v is the vacuum expectation value of the Higgs, the sum is over all fundamental charged particles, and N_{ci} and q_i are the color factor and charge of each particle in the sum. The functions F_i depend on the spin of the particle and are given by

$$F_i(\tau) = \begin{cases} -2\tau[1+(1-\tau)g(\tau)] & \text{fermions} \\ 2+3\tau+3\tau(2-\tau)g(\tau) & W \text{ boson} \end{cases}$$

$$\text{where } g(\tau) = \begin{cases} \left[\arcsin(1/\sqrt{\tau})\right]^2 & \tau \geq 1 \\ -\frac{1}{4}\left\{\ln\left[\frac{1+\sqrt{1-\tau}}{1-\sqrt{1-\tau}}\right]-i\pi\right\}^2 & \tau < 1. \end{cases} \tag{3.7}$$

Fig. 12 shows $\Gamma(H\to\gamma\gamma)$ as a function of the Higgs mass, where a top quark mass of 150 GeV is assumed.

Since an intermediate mass Higgs is a very narrow resonance ($\Gamma_T \approx$ few MeV $<< M$), we may use

$$\frac{1}{\pi}\frac{M\Gamma_T}{(W^2-M^2)^2+M^2\Gamma_T^2} \approx \delta(W^2-M^2), \tag{3.8}$$

so the number of Higgs $\to b\bar{b}$ events is given by

$$\begin{aligned} N_{H\to b\bar{b}} &= \left.\frac{dL_{\gamma\gamma}}{dW}\right|_M \frac{4\pi^2\Gamma(H \to \gamma\gamma)BR(H \to b\bar{b})}{M^2}(1+\lambda_1\lambda_2) \\ &\approx 1.54\times10^4\left(\frac{L_{ee}}{\text{fb}^{-1}}\right)\left(\frac{E_{ee}}{\text{TeV}}\right)^{-1}\left(\frac{\Gamma_{H\to\gamma\gamma}}{\text{keV}}\right)\left(\frac{M}{\text{GeV}}\right)^{-2}BR(H \to b\bar{b})F(M)(1+\lambda_1\lambda_2), \end{aligned} \tag{3.9}$$

where $F(M) = \frac{E_{ee}}{L_{ee}} \frac{dL_{\gamma\gamma}}{dW}\Big|_M$ is dimensionless and of order 1. The $H \to b\bar{b}$ branching ratio is plotted in Fig. 12. At a Higgs mass of ~120 GeV the $H \to WW^*$ width begins to be appreciable, so the $b\bar{b}$ branching ratio declines.

Photon polarization can play a crucial role in background (continuum $b\bar{b}$ production) suppression. Far above $b\bar{b}$ production threshold, the continuum cross section goes as

$$\frac{d\sigma_c(\gamma\gamma \to b\bar{b})}{d\cos\theta} \sim \frac{1+\cos^2\theta}{1-\cos^2\theta}(1-\lambda_1\lambda_2) \quad \text{for } \beta \to 1\ , \tag{3.10}$$

while Higgs production goes as $(1+\lambda_1\lambda_2)$. Choosing PLC machine parameters to enforce highly polarized photon beams (in the mass region of interest) and arranging for the colliding beams to have the same polarization significantly reduces the background while enhancing the signal. A cut on $\cos\theta$ also improves the signal-to-background ratio, since the continuum $b\bar{b}$ are preferentially produced at large dip angle ($|\cos\theta| \approx 1$), while the signal events are distributed uniformly in $\cos\theta$.

In order to study the ability of a PLC to search for an intermediate mass Higgs boson, the following method was utilized. A Monte Carlo event generator was used to produce $\gamma\gamma \to H \to b\bar{b}$ and continuum $\gamma\gamma \to b\bar{b}$ events using the $\gamma\gamma$ luminosity distribution (Eq. 2.23) and the cross sections of Eqs. 3.3–3.4. The $b\bar{b}$ partons were then fragmented into jets using JETSET 6.3 (LUND) [68] and the events processed through the Fast Monte Carlo Simulation of the SLD Detector. The resulting 'raw data' were then analyzed to try to detect the presence of a Higgs boson. The JADE [69] jet-finding algorithm was applied to the data and all two-jet events were kept as the final data sample. After a cut on the dip angle of the two jets (with both jets satisfying $|\cos\theta| < 0.9$) and a cut on the transverse jet-jet colinearity to reject badly measured events, a jet-jet invariant mass was formed. The presence of a 'bump' in a histogram of invariant masses would then signal the presence of a Higgs boson.

A note on the invariant mass reconstruction is due. A naïve reconstruction—simply adding the measured jet 4-momenta together and squaring—leads to a very poor invariant mass resolution; it is possible, by cleverly rescaling the jet 4-momenta before adding them, to improve the resolution significantly. After passing through the detector, many of the events have a fairly large measured value of p_T. This could be due to two causes: either the jet direction was badly measured (due to particles in the jet escaping down the beampipe or through a crack in the detector, for instance) or

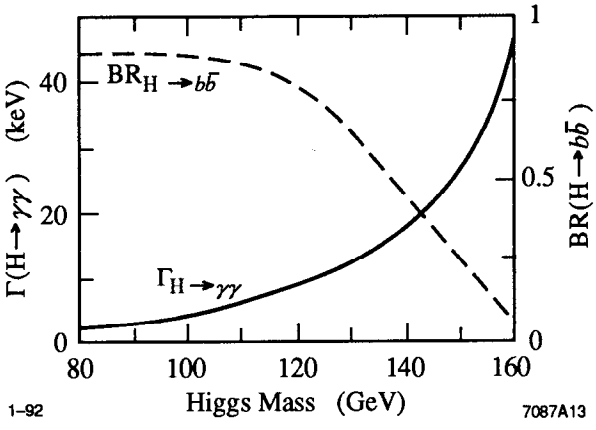

Fig. 12. Standard Model Higgs $\to \gamma\gamma$ partial width and Higgs $\to b\bar{b}$ branching ratio.

neutral particles in the jet were not detected by the calorimeter. In either case the resulting reconstructed invariant mass is too low. In the first case (mismeasured direction), there is not much that can be done except to reject the event. Only those events whose x–y jet projections were less than 10° from being back-to-back were kept in the event sample. Fortunately this rejects very few of the events which also pass the dip-angle cut ($|\cos\theta|$ of each jet < 0.9)—mismeasured direction simply is not much of a problem. Losing neutrals, however, is a significant problem, but also fortunately this problem can be partially remedied. Since the p_T arises because more neutrals escaped in one jet than in the other, before forming the jet-jet invariant mass one of the jet's 4-vectors is rescaled to balance p_T. As losing neutrals can never increase the measured momentum of a jet, the jet with the smaller value of p_T has its 4-momentum scaled upward so that the rescaled p_T matches that of the other jet. This improves the jet-jet invariant mass resolution by a factor of two. This method of improving jet-jet mass resolution is similar in spirit to the one used by Baltay et al. in Ref. [70].

It should be noted that no $b\bar{b}$ flavor tagging was simulated in the analysis; we unrealistically assumed 100% $b\bar{b}$ flavor tagging efficiency and no contamination of the $b\bar{b}$ sample by other flavors of quark (e.g., $c\bar{c}$). Although the assumption of 100% efficiency is optimisic, it is not yet clear how well one can do $b\bar{b}$ flavor tagging. Use of present methods implies that 40% to 50% $b\bar{b}$ flavor tagging efficiency is possible without significant contamination by other quark species, but research in this area is ongoing, and it is possible that much higher efficiencies are achievable [71-73]. In any case, such an assumption does not significantly affect the conclusions to be drawn from this study. If ultimately it is found that 50% tagging efficiency is the best one can do, our results would remain unchanged except that the integrated luminosites we quoted would need to be multiplied by two.

With regard to the choice of particular machine parameters, we demonstrate a search for an intermediate mass Higgs boson in the following manner: we first consider a collider in the limit of zero conversion distance (the laser beam intersects the linac beam close enough to the interaction point so that we may ignore the backscattered photon's angular divergence) and study the effects of varying the electron polarization at $\sqrt{s}$ of 300 and 500 GeV; we then study the effect of moving the conversion point a finite distance from the interaction point. The particular parameters chosen are:

Case 1:

- Electron beams of 150 GeV with 50% and 90% right polarization;
- Laser beams of 2.06 eV and 100% right polarization;
- Higgs masses of 90 and 140 GeV;
- 10 fb^{-1} of integrated ee luminosity;

Case 2:

- Electron beams of 250 GeV with 50% and 90% right polarization;
- Laser beams of 1.24 eV and 100% right polarization;
- Higgs masses of 90 and 140 GeV;
- 10 fb^{-1} of integrated *ee* luminosity;

Case 3:

- Electron beams of 250 GeV, 90% right polarization, and a cylindrical Gaussian profile with sigma of 100 nm;
- Laser beams of 1.24 eV and 100% right polarization, converting at a distance of 4 mm, 8 mm, and 12 mm;
- Higgs mass of 90 and 140 GeV;
- 20 fb^{-1} of integrated *ee* luminosity.

As noted earlier, we use a luminosity distribution which assumes each electron scatters exactly once in the laser photon pulse. The overestimation in the $\gamma\gamma$ luminosity distribution this assumption introduces is compensated for by assuming the conservative values of the integrated *ee* luminosity given above.

The results are displayed in Figs. 13–15. At $\sqrt{s}$ of 300 GeV (Fig. 13), a clear Higgs signal emerges above the continuum background for both 50% and 90% linac electron polarization, but the advantage of the higher e^- polarization is obvious: the ensuing higher degree of photon polarization greatly reduces the continuum background, enhancing the significance of the Higgs signal. As the energy of the *ee* collider is increased to 500 GeV (Fig. 14), two important effects are evident. The first is that signal-to-background improves, because the Higgs lies 'further back' on the photon polarization curve, resulting in a higher mean helicity product even at moderate linac electron polarizations. The second effect is a noticeable reduction in rate. This is due to two causes: first, as the total machine energy increases, the luminosity per unit mass interval decreases (the photon collisions are spread out over a greater energy range); second, the final state jets tend to be more boosted along the beam line, resulting in a lower fraction of the events in the detector. At machine energies above 500 GeV there is little further advantage from increased photon polarization, and the event rate begins to drop precipitously. It is for this reason that a moderate energy machine is favored for purposes of searching for the intermediate mass Higgs. If highly polarized electron beams are obtainable and a laser of the appropriate frequency range is available, then an *ee* machine with center-of-mass energy near 300 GeV seems most desirable; if only moderate electron polarization is possible, then a 500 GeV machine would be indicated.

As the conversion distance is increased (from 4 mm to 12 mm for a spotsize of 100 nm; see Fig. 15), the low-end luminosity decreases (recall that the lowest energy photons scatter at the highest angles from the beam-line and so do not contribute much to the luminosity). The result is a decreased event rate at low invariant mass, with a corresponding drop in the statistical significance of the 90 GeV Higgs signal. It is obvious that small conversion distances will need to be employed in order to ensure sufficient luminosity at low (~90 GeV) invariant mass. This will pose challenging questions for the design of the interaction region.

It should be noted that the results presented may be considered conservative, as the detectors which will be available for the next generation of linear collider will have considerable advantages over the SLD detector we use in our study. Primarily, better momentum resolution and greater calorimeter depth and segmentation will significantly improve the invariant mass resolution, allowing for a much greater signal-to-background ratio.

For a Higgs boson nearly degenerate with the Z there are additional backgrounds we have heretofore not considered. These backgrounds represent the production of a $Z + X$ final state with 'X' going undetected and the Z decaying to a $b\bar{b}$ pair. Before discussing these backgrounds, it should be noted that resonant production of a Z (i.e., $\gamma\gamma \rightarrow Z$) is *not* a background to $\gamma\gamma \rightarrow H$. By Bose symmetry, two massless spin-one objects do not couple to a spin-one resonance, a result known as the Yang-Landau theorem [74]. Consequently, the coupling of the Z to two real photons is identically zero. This is an important advantage of a PLC.

Two potential backgrounds which might fake the presence of a 90 GeV Higgs boson are: (1) $\gamma\gamma \rightarrow \gamma Z$, with the photon disappearing down the beam pipe and the Z decaying to $b\bar{b}$; and (2) $\gamma\gamma \rightarrow ZZ \rightarrow \nu\bar{\nu}b\bar{b}$. Fortunately, the cross sections for both these processes should be very small. The processes are fourth order in the coupling, so we expect the cross section to go as α^4/W^2 ($\simeq$ 0.15 fb at W = 100 GeV), more than two orders of magnitude smaller than the Higgs production cross section. We conclude that γZ and ZZ production do not constitute a serious background to a 90 GeV Higgs signal.

The most important background faking the presence of a 90 GeV Higgs is not a two-photon background, but rather is due to the presence of the residual electrons left over from the original Compton backscatter. Recall that if these electrons are not deflected following conversion, then they follow very nearly their original path and so intersect the oncoming high energy photon beam at the interaction point. The process $e\gamma \rightarrow eZ$ is then possible, and the final state electron is preferentially backscattered down the beam pipe, where it goes undetected. If the Z then decays to $b\bar{b}$, the event mimics a 90 GeV Higgs event. Monte Carlo studies show that the event rate for this process is two to three orders of magnitude larger than that from Higgs production. In order to minimize this background, it will be essential to displace the residual electrons far enough from the interaction point so as to reduce the $e\gamma$ luminosity by several orders of magnitude.

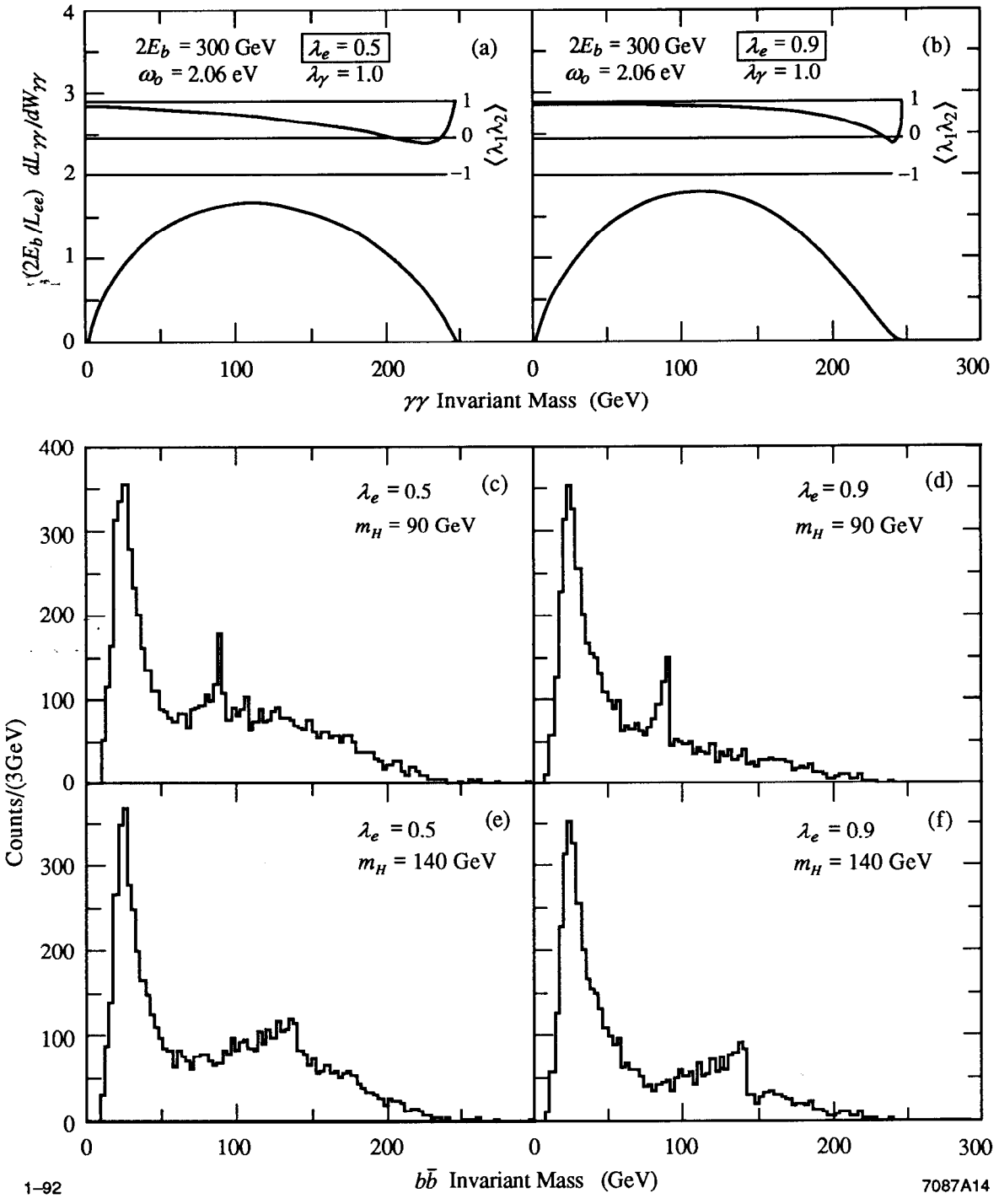

Fig. 13. The search for an intermediate mass Higgs boson at a $\gamma\gamma$ collider: Case 1. At an *ee* machine energy of 300 GeV, ignoring the effect of a finite conversion distance, and imposing a cut restricting each jet to $|\cos\theta| < .9$, a clear Higgs signal (for Higgs masses of 90 and 140 GeV) appears. 10 fb^{-1} of integrated effective *ee* luminosity is assumed, representing 1 'year' (10^7 sec) of running at 10^{33} cm^{-2} s^{-1}. The effect of using two different values of the linac electron polarization is demonstrated. The superior background suppression (arising from the higher degree of photon polarization) associated with the higher value of the electron polarization is obvious.

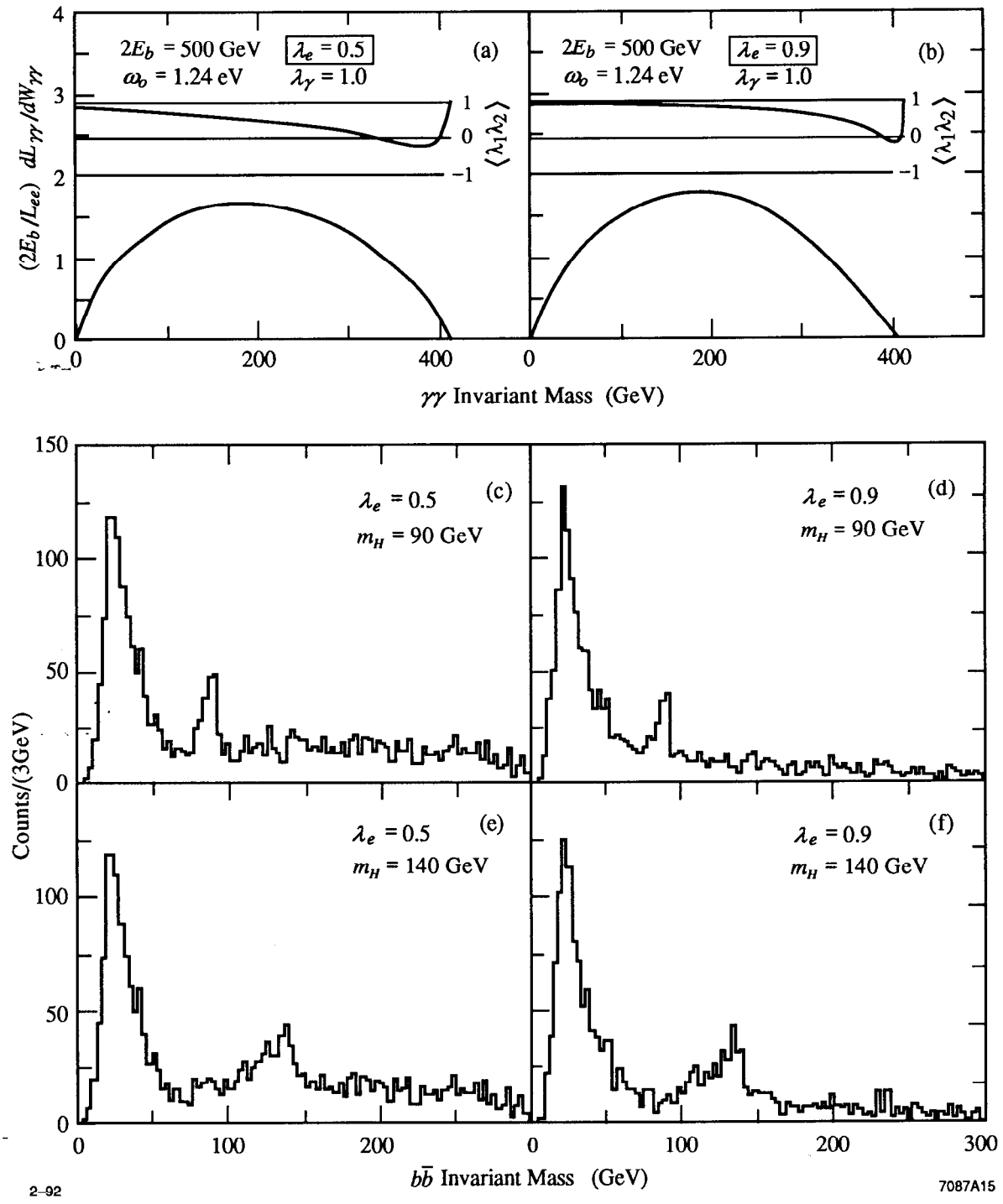

Fig. 14. The search for an intermediate mass Higgs boson at a $\gamma\gamma$ collider: Case 2. At an ee machine energy of 500 GeV (again ignoring the effect of a finite conversion distance, imposing a $|\cos\theta| < .9$ cut, and with 10 fb^{-1} of integrated luminosity) one distinct advantage and one distinct disadvantage of this higher energy machine over the 300 GeV case are apparent. The higher machine energy means that the Higgs boson lies 'further back' on the photon helicity curve, resulting in a high degree of photon polarization for lower linac electron polarization values, and therefore enhanced signal to noise. The event rate, however, is significantly lower at this energy than at 300 GeV, for two reasons: as the machine energy increases, the luminosity per unit mass interval decreases accordingly; also, as the machine energy increases, the amount by which the final state is boosted along the beamline increases, resulting in a lower fraction of the events in the detector.

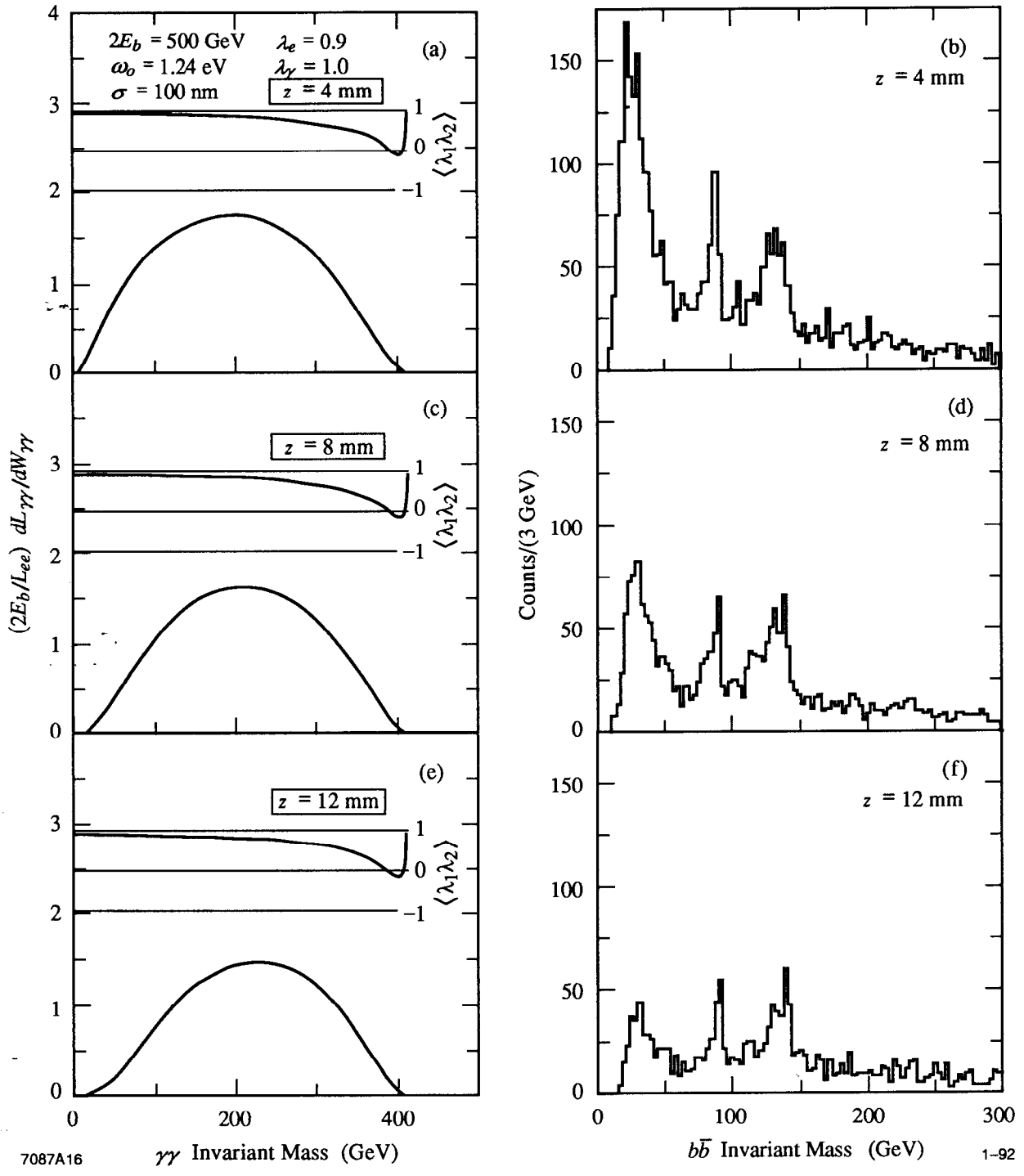

Fig. 15. The search for an intermediate mass Higgs boson at a $\gamma\gamma$ collider: Case 3. At an *ee* machine energy of 500 GeV with linac electron polarization of 90%, the effect of moving the conversion point back from the interaction point is demonstrated. A cylindrical electron beam with gaussian profile and σ of 100 nm is assumed, and conversion distances of 4, 8, and 12 mm are considered. Higgs masses of 90 and 140 GeV are both displayed in each plot. As the conversion distance is increased, the drop in luminosity (especially at 90 GeV) is apparent, and the significance of the signal is reduced accordingly. The same $|\cos\theta| < .9$ cut has been applied but note that an integrated luminosity of 20 fb^{-1} is assumed, twice that of Figs. 13 and 14.

In looking at Fig. 11, one might conclude that beamstrahlung photons offer a more attractive method of searching for the Higgs with mass less than about $0.3\sqrt{s}$, as the $\gamma\gamma$ luminosity is greater for beamstrahlung photons than for laser backscattered photons. The removal of the electrons from the interaction point, however, is impossible when using beamstrahlung photons, and so the ability to discover a Higgs with a mass near 90 GeV is lost.

2. $\gamma\gamma \rightarrow$ Higgs: Study

While a $\gamma\gamma$ collider serves as an attractive alternative to e^+e^- and hadron colliders in the search for a Higgs boson in the intermediate mass range, perhaps the most compelling argument for a PLC is its singular ability to study a Higgs boson once it is found [17]. After the discovery of a Higgs boson, it will be paramount to try to learn as much about it as is possible. One of the most important properties to determine is the Higgs partial width to two photons: recall that the coupling of the Higgs to $\gamma\gamma$ proceeds through loops of charged particles which couple to the Higgs, so the two-photon width is a sensitive probe of physics beyond the Standard Model [19]. Supersymmetric models, technicolor models, and other extensions of the Standard Model with more complicated Higgs sectors all predict two-photon couplings which are, in general, different from that of the Standard Model [29,75]. As an example we consider the Higgs-to-$\gamma\gamma$ partial width for an extension to the Standard Model with two Higgs doublets, where the up-type quarks couple to one doublet while the down-type quarks couple to the other [29]. Plotted in Fig. 16 is the ratio of $\gamma\gamma$ partial widths in this two-Higgs doublet model to that in the Standard model. The ratio of partial widths is given as a function of $\tan\beta$, the ratio of Higgs vacuum expectation values (v_u/v_d), at various values of α, the neutral Higgs mixing angle, for representative values of the Higgs' masses. The $\gamma\gamma$ width differs significantly from the Standard Model value.

A $\gamma\gamma$ collider provides a unique opportunity to measure the two-photon width of a Higgs boson. We have heretofore stressed the broad luminosity distribution attainable at a PLC, but it is also possible (and in practice much easier) to attain a more monochromatic 'peaked' luminosity distribution. The machine can be designed so that the peak of the distribution 'sits' on the Higgs resonance. As an example we assume that

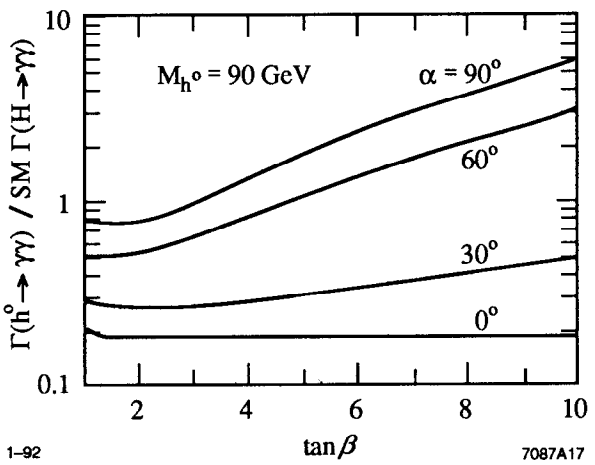

Fig. 16. The Higgs (h^o) $\rightarrow \gamma\gamma$ partial width in an extension to the Standard Model with two Higgs doublets, for M_{h^o} = 90 GeV. Tanβ is the ratio of Higgs vacuum expectation values, and α is the neutral Higgs mixing angle; the other physical Higgs bosons are assigned the following masses: $M_{H^\pm}$ = 100 GeV; M_{A^o} = 300 GeV; M_{H^o} = 500 GeV. The partial width is normalized to the Standard Model value.

a Higgs with a mass of 90 GeV has been discovered; PLC parameters similar to those shown in Fig. 17 (a) could then be used to study it. Assuming an integrated luminosity of 10 fb^{-1} and a Standard Model Higgs boson, Monte Carlo simulations indicate an expected 500 Higgs events over a background of 200 continuum $b\bar{b}$ events (with $|\cos\theta| < 0.8$), allowing a determination of the two-photon width to within 6%. If a 140 GeV Higgs were to be discovered, a machine with the parameters of Fig. 17(b) could be used. With 10 fb^{-1} of integrated luminosity, we would expect nearly 600 Higgs events above 70 continuum $b\bar{b}$ events, allowing a determination of the two-photon width to within 5%.

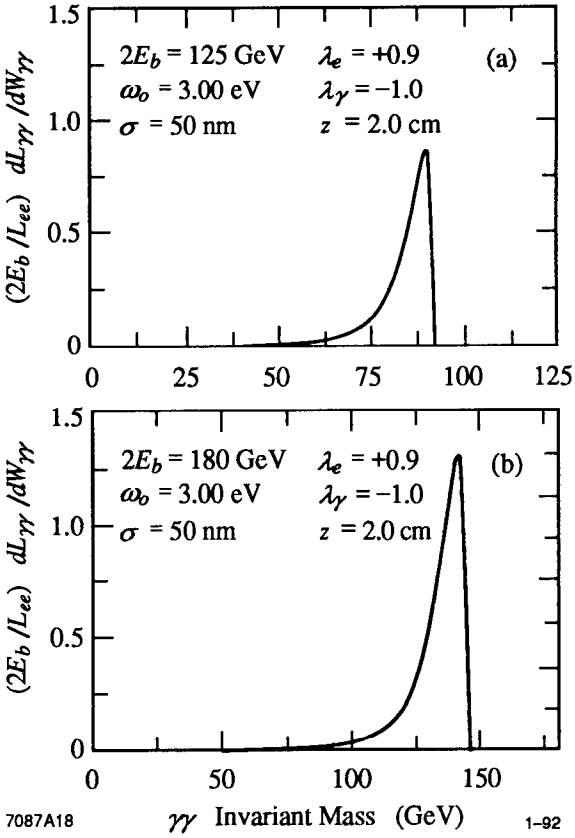

Fig. 17. The luminosity distribution of a $\gamma\gamma$ collider designed to study (a) a 90 GeV or (b) a 140 GeV Higgs boson.

3. Heavy Higgs Production

While Higgs bosons with masses above $2M_Z$ should be readily discovered at the SSC or LHC, it will still be of considerable interest to measure the rare 2γ decay mode width. This may best be done by studying the reaction $\gamma\gamma \to H \to ZZ$ [30,76]. Alternatively, one could examine the process $e\gamma \to W\nu H$ ($H \to ZZ$ or WW) [77,78]. For a sufficiently high $\sqrt{s}$ PLC, these reactions should allow a measurement of the two-photon coupling of the Higgs for a Higgs mass up to at least 500 GeV.

B. Searches for New Particles

A PLC also serves as an excellent machine with which to search for new particles. Heavy charged particles (such as charged Higgs bosons or charged superpartners) are an obvious example, produced through $\gamma\gamma \to X^+X^-$, but photo-production of charged particle pairs does not differ fundamentally from pair production in e^+e^- annihilation, so we reserve discussion of such processes until the end of this section. Rather, the unique contribution a $\gamma\gamma$ collider can make in the search for new particles is in looking for particles with an appreciable coupling to two photons.

As an $e\gamma$ collider a PLC also holds unique advantages in the search for new particles. An $e\gamma$ initial state is qualitatively different from an e^+e^- or proton-antiproton initial state, so an $e\gamma$ collider provides an opportunity to study physics generally inaccessible at conventional colliders.

We discuss in detail two of these processes, a search for excited electron states (e^*) to test for electron compositeness and a search for supersymmetry via the production of $\tilde{e}\tilde{\gamma}$ pairs. In both cases we consider full helicity amplitudes and denote by λ_e and λ_γ the helicities (= ± 1) of the colliding electron and photon.

1. $\gamma\gamma \to X \to \gamma\gamma$

In addition to allowing the search for an intermediate mass Higgs boson, a PLC is also suited to the discovery of other resonances in $\gamma\gamma$ collisions. Since e^+e^- colliders produce particles as resonances with charge conjugation C = −1, while a $\gamma\gamma$ collider would produce C = +1 particles, the two searches are complementary. For any particle decaying to two photons, the $\gamma\gamma$ collider provides a unique discovery channel. As an example of such a particle, we take the η-like particle composed of color sextet quarks proposed by Kang and White (the η_6 in their nomenclature) to explain the large value of the real part of the forward $p\bar{p}$ elastic scattering amplitude, the decays of which may also be the source of the mini-Centauro and Geminion cosmic ray events [79]. This particle would have a mass of about 30 GeV and would decay primarily to two photons, with a two-photon width of ~140 eV. Our Monte Carlo studies indicate that 10 fb^{-1} of integrated luminosity at a machine with E_{ee} = 300 GeV would result in about 100 events (in the detector) in a distinctive peak above a small, falling background, making the discovery and study of this particle a simple task.

A further example is that of neutral Higgsonium, a C = +1 bound state of Higgs bosons in a strongly interacting theory, proposed by Grifols in Ref. [80]. Following his example, we assume a 200 GeV Higgsonium state consisting of an H^+H^- pair bound by exchange of neutral Higgs with mass of 50 GeV, in a strongly interacting Higgs sector with two Higgs doublets. Such a state has a two-photon width of 2.73 MeV and decays primarily to W pairs, but decays to two photons approximately 0.17% of the time. Concentrating on the $\gamma\gamma$ decay channel and assuming an ee machine with $\sqrt{s}$ = 500 GeV, Monte Carlo studies indicate 105 events after 10 fb^{-1} of integrated luminosity. Again, the signal events form a narrrow peak above a very small, falling background; discovery and study of this state would also be particularly easy. Even better, in $\gamma\gamma \to$ Higgsonium $\to W^+W^- \to$ 4 jets, the Higgsonium state would stand out as a clear resonance. Assuming a 4-jet invariant mass reconstruction resolution of ~10 GeV, there would be about 3400 events/fb^{-1} in a peak above a smooth $\gamma\gamma \to W^+W^- \to$ 4 jet background of approximately 1000 events/fb^{-1}.

Other examples abound in the literature. Renard [81] has considered the probability of producing non-standard scalar particles in $\gamma\gamma$ reactions at $\sqrt{s}$ = 500 GeV and finds this process has a much greater mass reach than pair production from e^+e^- annihilation. Many authors have

considered axion production in $e\gamma$ collisions [82,83] or $\gamma\gamma$ collisions [84,85]; these usually require a very low energy facility and will not be discussed here.

2. $e\gamma \to e^* \to e\gamma$

In considering physics beyond the Standard Model, it is often conjectured that some of the particles we now consider fundamental are in fact composite objects—the 'hadrons' of some more fundamental theory. The most popular of these models—technicolor—assumes a composite Higgs boson [38], but others assume composite W and Z particles or composite quarks and leptons [36,86,87]. One of the most testable predictions of the latter of such theories is the proposed existence of excited states of the electron. Experiments in the past sought such states through production of ee^* and e^*e^* in e^+e^- collisions, leading to a lower limit on masses of 44.6 GeV (95% CL) [32]. Future e^+e^- machines should be able to extend these searches to much higher masses, but a PLC offers the opportunity for a particularly clean discovery channel: at an $e\gamma$ collider it becomes possible to search for such states as resonances in $e\gamma$ (Compton) scattering [88–90].

We take as our model the following C-invariant interaction lagrangian:

$$L_{\text{int}} = \frac{e\eta}{2M}\overline{\psi}_{e^*}\sigma^{\mu\nu}(1+i\gamma_5)\psi_e F_{\mu\nu} + \text{ h.c.}, \tag{3.11}$$

where η is a (dimensionless) coupling constant and M is the e^* mass [9]. Assuming the e^* is a narrow resonance ($\Gamma << M$), we may ignore interference effects between the (u and t channel) continuum diagrams and the (s channel) resonance diagram,[1] so that the cross section decomposes into sum of a Compton scattering cross section and an e^* Breit-Wigner cross-section [9]:

$$\sigma(e\gamma \to e\gamma) = \sigma_c(e\gamma \to e\gamma) + \sigma(e\gamma \to e^* \to e\gamma) \tag{3.12}$$

$$\frac{d\sigma_c(e\gamma \to e\gamma)}{d\cos\theta} = \frac{\pi\alpha^2}{2W^2}\left[\frac{4}{1+\cos\theta+2\frac{m_e^2}{W^2}}(1+\lambda_e\lambda_\gamma)+(1+\cos\theta)(1-\lambda_e\lambda_\gamma)\right] \tag{3.13}$$

$$\sigma(e\gamma \to e^* \to e\gamma) = \frac{8\pi\Gamma(e^* \to e\gamma)^2}{(W^2-M^2)^2+M^2\Gamma_T^2}(1+\lambda_e\lambda_\gamma), \tag{3.14}$$

where θ is the electron scattering angle and the $e^* \to e\gamma$ width is given by

$$\Gamma(e^* \to e\gamma) = \alpha\eta^2 M. \tag{3.15}$$

[1] We also ignore the enhancement of the continuum cross section due to virtual e^* effects.

In the narrow-width approximation,

$$\frac{1}{\pi}\frac{M\Gamma_T}{(W^2-M^2)^2+M^2\Gamma_T^2} \approx \delta(W^2-M^2), \tag{3.16}$$

so the number of e^* events expected is

$$\begin{aligned} N_{e^*\to e\gamma} &= \left.\frac{dL_{e\gamma}}{dW}\right|_M \frac{4\pi^2\Gamma(e^*\to e\gamma)BR(e^*\to e\gamma)}{M^2}(1+\lambda_e\lambda_\gamma) \\ &\approx 10^5\left(\frac{L_{ee}}{\text{fb}^{-1}}\right)\left(\frac{E_{ee}}{\text{TeV}}\right)^{-1}\left(\frac{M}{\text{TeV}}\right)^{-1} F(M)\eta^2 BR(e^*\to e\gamma)(1+\lambda_e\lambda_\gamma), \end{aligned} \tag{3.17}$$

where $F(M) = \frac{E_{ee}}{L_{ee}}\left.\frac{dL_{e\gamma}}{dW}\right|_M$ is dimensionless and of order 1.

Observance of the e^* as a resonance in the $e\gamma$ invariant mass distribution will of course depend on the resolution of the detector used, as well as on values of the e^* coupling, mass, and width. As a specific example we assume the following parameters:

- a parent collider with one 200 GeV beam, the colliding beam, and one 250 GeV beam, the beam used to convert laser photons to high energy photons (the asymmetry in electron beam energies ensuring that the highest energy $e\gamma$ collisions occur in the center-of-mass), each unpolarized and with a cylindrical Gaussian profile with sigma of 100 nm;
- unpolarized laser photons of 1.24 eV (implying $x = 4.75$) converting at a distance $z = 4$ mm (to ensure a broad luminosity distribution);
- three different e^* masses of 100, 200, and 300 GeV, each with a coupling $\eta = 0.1$ and branching ratio to $e\gamma$ of 0.5.

The choices of coupling ($\eta = 0.1$) and branching ratio (BR = 0.5) are completely arbitrary but are made with the following prejudice: η is chosen to be of order unity but small enough so as not to exaggerate the production of excited electrons, and the decays are chosen evenly split between electromagnetic and weak modes.

We employ a Monte Carlo simulation of the SLD detector to provide a realistic approximation to real data; it should be noted that the SLD detector has a conventional magnetic coil and only average charged particle momentum resolution—it may safely be assumed that the true detector employed at a PLC will do significantly better, especially at high momentum.

As the Compton cross section is peaked strongly in the backward direction, we cut all events in which the electron is measured with $\cos\theta < -0.7$. We also reject badly measured events by cutting on missing p_T: all events with missing $p_T > 10$ GeV are rejected. This cut significantly reduces the e^* tails without affecting the number of events in the peak.

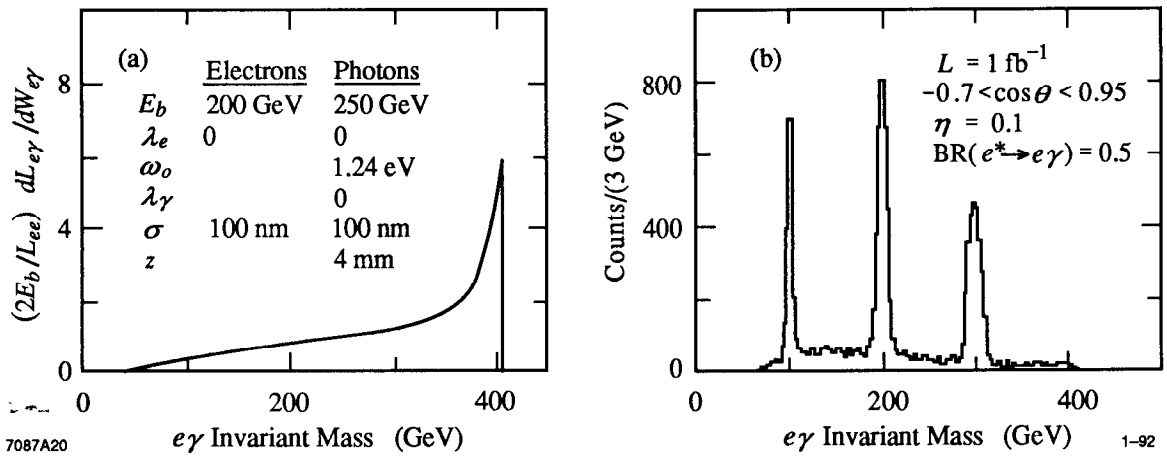

Fig. 18 (a) $e\gamma$ luminosity distribution for a PLC with the given machine parameters. (b) $e\gamma$ invariant mass distribution. The background curve is from conventional Compton scattering, the peaks arise from the presence of three excited electron states at masses of 100, 200, and 300 GeV. The cut on $\cos\theta$ refers to the electron scattering angle, and there is an additional cut of 10 GeV on missing p_T.

Figure 18 shows the $e\gamma$ luminosity distribution arising from the given machine parameters, and the resulting $e\gamma$ invariant mass distribution, with all e^* masses plotted on the same histogram, assuming an integrated luminosity of 1 fb^{-1}. For a conservative ee luminosity of 10^{33} cm^{-2} sec^{-1}, this represents a few weeks of data collection. It is obvious that given a reasonable e^* coupling and $e\gamma$ branching ratio, and mass less than almost the full machine energy, an excited electron state will easily be discovered in an $e\gamma$ collider.

We have chosen to use unpolarized beams, as polarization effects tend to be rather model dependent [9]. If an excited electron state is discovered, however, varying the electron and photon polarization would serve as an excellent way to study such a state.

3. $e\gamma \to \tilde{e}\tilde{\gamma}$

Supersymmetry is perhaps one of the most compelling ideas to hit particle physics since the dawn of gauge theories and the Standard Model. In addition to necessitating an extended Higgs sector, supersymmetry also predicts the existence of new particles: each particle in the Standard Model must be accompanied by a partner with identical mass and quantum numbers, save for spin, which must differ by one-half unit (a fermion-boson symmetry) [26,27]. Although supersymmetry must be a broken symmetry, since no degenerate partners of any known particles have been observed, it should be broken at the weak scale in order to serve as a solution to the hierarchy problem, leaving the superpartner masses in the 10's to 100's of GeV range [31]. The search for such superpartners promises to be one of the most important endeavors in particle physics over the next decades.

An $e\gamma$ collider provides a particularly clean environment to search for the superpartner of the electron (dubbed the selectron) through production of a selectron-neutralino pair. The superpartners of the photon, Z, and Higgs bosons (at least two Higgs doublets being required by supersymmetry) are named the photino, zino, and Higgsinos, but in general the mass eigenstates of the superpartners are not the interaction eigenstates, so the generic term 'neutralino' is given to the linear combinations which have definite mass. Most supersymmetric models require that the lightest of the neutralinos, the Lightest Supersymmetric Particle (LSP), be stable. While the production cross section—and subsequent selectron decay—is model (mass and mixing angle) dependent, we have chosen a somewhat unrealistic but simple and illustrative case: we have assumed that the LSP is pure photino, and that the selectron decays 100% of the time to an electron and the LSP. This allows the search for supersymmetry through the process $e\gamma \to \tilde{e}\tilde{\gamma} \to e\tilde{\gamma}\tilde{\gamma}$.

The selectron is short lived and decays at the interaction point to an electron and an additional photino. As our photino is the LSP, it is stable and only weakly interacting, so both photinos escape the detector. The signature for selectron-photino production is then a single electron in the detector, with substantial missing energy. We assume an interaction Lagrangian as given by Haber and Kane in Ref. [27]. The $\tilde{e}\tilde{\gamma}$ production cross-section is then given by

$$\begin{aligned}
\frac{d\sigma(e\gamma \to \tilde{e}_L\tilde{\gamma})}{d\cos\theta} &= \frac{\pi\alpha^2}{4W^2}(1-\lambda_e)(1+\delta)\rho \\
&\quad \times \left\{1-\delta-\rho(1+\delta)\cos\theta + 4\delta\left(\frac{2(\sigma+\delta)}{(1+\delta)^2}-1\right)\frac{1-\cos^2\theta}{(1+\rho\cos\theta)^2}\right. \\
&\quad \left. +\lambda_\gamma\left[1+3\delta-\rho(1+\delta)\cos\theta - 4\frac{\sigma+\delta}{1+\delta}\frac{1}{1+\rho\cos\theta}\right]\right\} \\
\frac{d\sigma(e\gamma \to \tilde{e}_R\tilde{\gamma})}{d\cos\theta} &= \frac{d\sigma(e\gamma \to \tilde{e}_L\tilde{\gamma})}{d\cos\theta}\ (\lambda_e \to -\lambda_e\ ,\ \lambda_\gamma \to -\lambda_\gamma),
\end{aligned} \tag{3.18}$$

where $\delta \equiv (m_{\tilde{e}}^2 - m_{\tilde{\gamma}}^2)/W^2$, $\sigma \equiv (m_{\tilde{e}}^2 + m_{\tilde{\gamma}}^2)/W^2$, $\rho \equiv p/E = \sqrt{1+\delta^2-2\sigma}/(1+\delta)$, and θ is the selectron scattering angle with respect to the original electron direction [9].

There are three primary backgrounds with which to be concerned: Compton scattering ($e\gamma \to e\gamma$), where the photon escapes down the beampipe or through a crack in the detector; $e\gamma \to eZ \to e\bar{\nu}\nu$; and $e\gamma \to W\nu \to e\bar{\nu}\nu$. It is this last background which is most important. In the first two backgrounds the electron typically has very nearly half the total event energy, whereas in the SUSY signal events and the W background events the electron typically has much less than half the event energy. Recall, though, that the $e\gamma$ luminosity is not totally monochromatic, so that some $e\gamma$ or eZ events may have less than half the total energy, and do serve as a legitimate background.

The Compton cross section was given in Eq. 3.13. The eZ production cross section is [9]

$$\frac{d\sigma(e\gamma \to eZ)}{d\cos\theta_e} = \frac{\pi\alpha^2}{2W^2} \frac{1}{1+\cos\theta_e + \frac{2m_e^2}{W^2(1-r)^2}} \times \left\{ \left[c_1(1-\lambda_e\lambda_\gamma) - c_2(\lambda_e - \lambda_\gamma) \right] \left[1+r+(1-r)\cos\theta_e \right]^2 + \left[c_1(1+\lambda_e\lambda_\gamma) - c_2(\lambda_e+\lambda_\gamma) \right] 4(1-r)^2 \right\}, \quad (3.19)$$

where $r = M_Z^2/W^2$, $c_1 = \frac{1-4\sin^2\theta_W+8\sin^4\theta_W}{8\sin^2\theta_W\cos^2\theta_W} \approx 0.36$, $c_2 = \frac{1-4\sin^2\theta_W}{8\sin^2\theta_W\cos^2\theta_W} \approx 0.07$, and θ_e is the electron scattering angle.

The $W\nu$ cross section is [15]

$$\frac{d\sigma(e\gamma \to W\nu)}{d\cos\psi} = (1-\lambda_e)\frac{\pi\alpha^2}{4W^2\sin^2\theta_W}\beta^4 \frac{\sum_{\lambda_W}\left|\Im_{\lambda_\gamma\lambda_W}\right|^2}{\left[2-\beta^2(1-\cos\psi)\right]^2}, \quad (3.20)$$

where $\beta = \sqrt{1-\left(M_W^2/W^2\right)}$, ψ is the W scattering angle (with respect to the original electron direction), and the $\left|\Im_{\lambda_\gamma\lambda_W}\right|$ are given by

$$\begin{aligned} |\Im_{--}|^2 &= 4\beta^4(1-\cos\psi) & |\Im_{+-}|^2 &= (1-\beta^2)^2(1+\cos\psi)\sin^2\psi \\ |\Im_{-0}|^2 &= 0 & |\Im_{+0}|^2 &= 2(1-\beta^2)(1-\cos\psi)\sin^2\psi \\ |\Im_{-+}|^2 &= 0 & |\Im_{++}|^2 &= (1-\cos\psi)^3. \end{aligned} \quad (3.21)$$

The selectron-photino production cross section is small, so care must be taken to reduce backgrounds, by a suitable choice of PLC machine parameters and by careful analysis. The $W\nu$ background is the most serious, but $W\nu$ production can be actively suppressed by colliding a beam of right-handed electrons, which do not couple to W^-'s. This necessarily limits the SUSY search to right-selectrons.

To illustrate a selectron-photino search at an $e\gamma$ collider, we choose the following PLC machine parameters:

- a colliding beam energy of 400 GeV with a cylindrical Gaussian profile having sigma of 50 nm and mean electron polarization of +90%;
- a converting beam energy of 500 GeV with a cylindrical Gaussian profile having sigma of 50 nm and mean electron polarization of –90%;
- a laser beam of frequency 0.62 eV and polarization +100%;
- a conversion distance (z) of 5 cm.

Figure 19(a) displays the resulting luminosity distribution.

In order to enhance the signal above background, it is necessary to make kinematic cuts in the final event selection. All three background processes tend to produce electrons directed in the backward direction, while the signal events tend to have the electron angle more evenly distributed in $\cos\theta$; thus a cut of -0.4 in the $\cos\theta$ of the final state electron is applied. The Compton background (with an undetected photon) is the most difficult to get a handle on, as its importance is strongly dependent on the specifics of the detector employed. In order to be sure we have accounted for this background, we make an additional cut of $\cos\theta < 0.9$. In Monte Carlo studies, no Compton scattering event with a photon within 15° of the beam pipe (which might have gone undetected) left an electron which passed both of the above cuts ($-0.4 < \cos\theta < 0.9$).

For this study, no detector simulation was employed, as the SLD detector simulation is unreliable at the energies we considered (~ few hundred GeV electrons). This should not much affect the results, as fine momentum resolution is unimportant for this process, and as the final state is such a simple one (a lone electron in the detector).

Figure 19 displays the electron energy distribution for various choices of the selectron and photino masses. The uppermost line in each plot is the total spectrum; the shaded region represents the signal ($\tilde{e}\tilde{\gamma}$ production) above the background ($W\nu$ and eZ events). The peak at ~400 GeV is from eZ production with the Z disappearing into the neutrino decay channel; the peak at low energy is from $W\nu$ production, where the W is right polarized and emits the electron in the direction opposite to its velocity. For electron energies between 40 and 340 GeV, there are relatively few background events, whereas the majority of the signal events lie in this region. For the model we have chosen, the signal is clear above the background; a more realistic model, in which the LSP is not pure photino or in which the selectron has additional decay channels, would lead to a reduction in the signal. However, unless the LSP has little photino contribution, the signal would still be apparent.

4. Further Discovery Potential in $e\gamma$ Collisions

We mention in passing that Renard has considered a number of possible discovery channels produced by $e\gamma$ collisions, such as $e\gamma \rightarrow [eb^o, f^-b^o, eb^+b^-, ef^+f^-]$, where b is a boson and f a fermion [9]. The Kang-White particle mentioned above could also be produced in association with an electron in this way, through a collision of a virtual bremsstrahlung photon with a real photon. Indeed, the $e\gamma$ and $\gamma\gamma$ 'two-photon' processes are complementary in that $\gamma\gamma$ utilizes two real photons, while $e\gamma$ requires one real and one virtual photon and hence can produce spin-one resonances, forbidden in the $\gamma\gamma$ case [74].

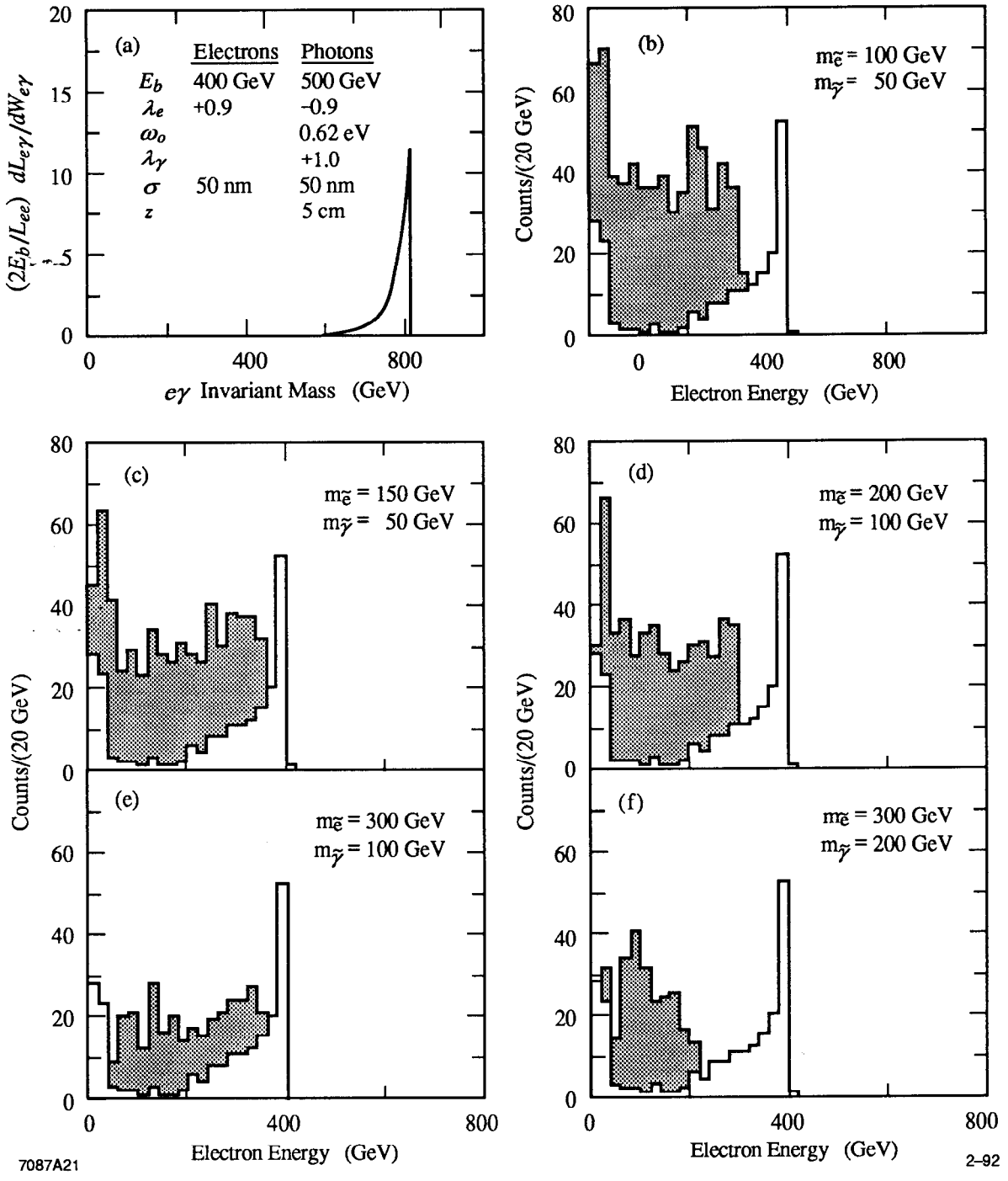

Fig. 19. Electron energy distribution for single electron events in $e\gamma$ collisions. Modeled are three processes $e\gamma \to W\nu \to e\bar{\nu}\nu$, $e\gamma \to eZ \to e\bar{\nu}\nu$, and $e\gamma \to \tilde{e}\tilde{\gamma} \to e\tilde{\gamma}\tilde{\gamma}$. The solid line is the total spectrum; the shaded regions represent the signal ($\tilde{e}\tilde{\gamma}$ production) above the background ($W\nu$ and eZ events). The peak at ~400 GeV is from eZ; the peak at low energy is from $W\nu$ production with a right polarized W emitting an electron in the direction opposite to the W's velocity. A cut of $-0.4 < \cos\theta < 0.9$ on the electron direction has been applied and an integrated luminosity of 10 fb^{-1} is assumed.

5. $\gamma\gamma \rightarrow X^+X^-$

While searches for heavy charged particles through $\gamma\gamma$ pair production are certainly viable at a PLC, such a machine does not seem to provide any particular advantage over e^+e^- colliders. The search for charged particle pairs such as charged Higgs or charged SUSY particles proceeds at a $\gamma\gamma$ collider in much the same way that it does at an e^+e^- collider [91]. While event rates at a PLC may be higher than at an e^+e^- collider, as the luminosity of a $\gamma\gamma$ collider can exceed that of e^+e^- colliders and as photo-production cross sections are 3 to 6 times larger than those in e^+e^- annihilation [8], the more monochromatic spectrum of e^+e^- machines leads to advantages in the final event analysis, resulting in a better invariant mass resolution than is possible at a $\gamma\gamma$ collider. What is most important to realize, however, is that a PLC designed for one of the other purposes outlined in this paper would also serve as a very good laboratory in which to search for new heavy charged particles.

C. Precision Electroweak Studies

A moderate energy linear collider built soon would be an excellent way to determine the properties of the W boson via $e\gamma \rightarrow W\nu$ and $\gamma\gamma \rightarrow WW$ [10-16]. Even if the obvious properties have been determined, these processes are an excellent way to test the vector-vector sector of the electroweak theory. In particular, the $WW\gamma$ vertex can be studied without the complicating effects of the γ-Z interference which occurs for the more commonly considered process $e^+e^- \rightarrow WW$ [92]. In this way anomalous electromagnetic moments of the W can be searched for, providing sensitivity to possible compositeness of the W, for example. The magnetic dipole moment μ and electric quadrupole moment Q of the W boson are characterized by two numbers, κ and λ, and are given by

$$\mu = \frac{e(1+\kappa+\lambda)}{2M_W}, \qquad Q = \frac{2e(\lambda-\kappa)}{M_W^2}, \tag{3.22}$$

where the Standard Model values are $\kappa = 1$ and $\lambda = 0$ [92].

While $e\gamma \rightarrow W\nu$ gives a virtually background-free event topology, $\gamma\gamma \rightarrow WW$ also is quite a clean process, and both give good and quite complementary determinations of κ and λ. Excellent comparisons of these two methods with $e^+e^- \rightarrow WW$ can be found in Refs. [14-16]. The latter process gives two ambiguous solutions in the κ–λ plane, which can be resolved by the $e\gamma$ or $\gamma\gamma$ measurement. In contrast, a measurement at the SSC could give a very good determination of λ, but has little sensitivity to κ [93]. Note that the sensitivities to κ and λ provided by e^+e^-, $e\gamma$, and

$\gamma\gamma$ colliders are roughly an order of magnitude better than those likely to be obtained at the Tevatron, LEP-II, or HERA [94].

Renard suggests also studying the process $e\gamma \rightarrow eZ$ to look for anomalous $\gamma\gamma Z$ and γZZ couplings, where the former could come from a composite Z or an additional spin-one composite particle [9,95,96].

D. Strong Interaction Studies

Two-photon physics, through virtual bremsstrahlung at e^+e^- storage rings, has already demonstrated considerable promise in the study of the quark model and QCD, allowing an exploration of the theory in the 1-2 GeV range [97]. Further work, however, will require extensions to energies in the ~10 GeV and ~100 GeV regimes. Many studies have already been done extending present results to the larger $\gamma\gamma$ center-of-mass energies (W) and virtual photon masses available at higher energy or luminosity machines, especially LEP-II [98], B Factories [99], HERA [100,101], and e^+e^- linear colliders [102]. A PLC provides an additional, and extremely powerful, tool for the study of the strong sector of the Standard Model via high energy collisions of both real photons (as a $\gamma\gamma$ collider) and virtual photons (as an $e\gamma$ collider) over the whole range of masses from ~10 to several hundred GeV. At first thought, it would appear that a PLC suitable for physics at energies of 100 to 1000 GeV would be of relatively little use at mass scales $\leq$ 10 GeV; as has been shown, however, tuning of the laser pulse intensity at a PLC to cause multiple interactions of electrons with laser photons would greatly enhance the resulting photon spectrum at relatively low energies, without loss of high energy photons. Thus, it seems appropriate to take a brief look at the physics which might benefit from the much higher W and Q^2 range and higher luminosities available at a PLC.

Experiments at relatively low energy e^+e^- colliders have measured the cross section for deep-inelastic $e\gamma$ scattering, where the γ is an off-shell virtual photon with mass $\sqrt{Q^2}$ radiated from one $e^\pm$ which interacts with the other $e^\pm$ via exchange of a nearly real photon [103]. However, the low available W and Q^2 range have allowed measurement only of one of the photon structure functions, F_2^γ, and in a regime where the photon still partly behaves like a hadron as described by vector dominance. Higher energies will allow a more direct comparison with QCD predictions of a log Q^2 rise in the structure functions (due to the running behavior of the coupling α_S), whose slope will be modified at very large Q^2 by the effects of gluon bremsstrahlung [104]. A high energy $e\gamma$ collider would be ideal for measurements at large x ($\equiv Q^2/(Q^2+W^2)$), and large Q^2, where those effects are maximal [105].

Additional information about the structure of photons and about QCD should be available from the study of jet and inclusive single-hadron production in $\gamma\gamma$ and $e\gamma$ collisions at high transverse momenta. In this kinematic regime, which is easily reached only with very high energy photons,

inclusive jet production should be as clean as in e^+e^- collisions, with a reaction rate one to three orders of magnitude larger [106]. In particular, jet cross sections and hard photon inclusive production should be sensitive to the gluon content of the photon, a quantity which is almost totally unknown at present [107]. The likelihood of interacting polarized photons with other photons or electrons should allow for detailed understanding of QCD amplitudes [108,109]. Although the study of these processes is possible at an e^+e^- collider using beamstrahlung photons [110], a PLC provides a cleaner environment and much higher energies than are available using beamstrahlung.

The study of exclusive hadron production in $\gamma\gamma$ and $e\gamma$ reactions has been the subject of much theoretical analysis dating to the days before there was any experimental data [111]. The arrival of measurements for hadron pair production and pseudoscalar meson production [112] has stimulated considerable new activity in this field [113]. However, the data have only begun to reach the kinematic regions for which solid QCD predictions can be made. The real strength of a high energy, high luminosity collider would be to make detailed measurements in these new regimes, where QCD must show itself capable of predicting the normalization as well as the shape of these cross sections. Measurement of basic processes like $e\gamma \rightarrow$ pseudoscalar can yield precise values for the QCD running coupling constant and detail the hadronic wavefunctions themselves [114]. Baryon structure, and the existence of four-quark states, will be accessible via $\gamma\gamma \rightarrow$ baryon+antibaryon. Meson pair production can be studied both in the light and heavy quark sectors, perhaps even including top-quark mesons for which non-relativistic quark model predictions should be quite accurate. An especially interesting process is $e\gamma \rightarrow \bar{t}b\nu$ which could be one of the few possible ways to measure directly the CKM matrix element V_{tb} [115].

There may be opportunities to study meson resonances at a PLC. The two-photon couplings of even-spin, C = +1 mesons can be measured in $\gamma\gamma$ reactions, while spin-1 mesons and meson form factors can be studied in $e\gamma$ reactions. The high energy of laser backscattered photons makes it difficult to work at the low masses required for light quark resonance production. Probably the easiest way to search for mesons made from u, d, and s quarks at a high energy linear collider is through either virtual bremsstrahlung or beamstrahlung photon interactions, since the photon fluxes are concentrated at relatively low energy. However, since a PLC would almost certainly be the first machine which can study C = +1 $b\bar{b}$ resonances in two-photon reactions, it will be more important to attempt to optimize the photon fluxes to give masses ~10 GeV. In the laser scheme this can be done by using a very intense laser pulse, leading to multiple scattering of the electrons in the laser pulse and large differential luminosities across the whole spectrum. Alternatively, one could also take advantage of the beamstrahlung spectrum normally present in a linear collider [116]. Such studies might even be possible at the SLC if suitable lasers can be developed soon. The $t\bar{t}$ C = +1 resonance structure would be well suited to a higher energy PLC [117]. Since it is

likely that the top quark is more massive than 90 GeV, however, it may decay too quickly (predominantly to Wb) to form well-separated resonances [118]. Higgs boson exchange, though, may still allow toponium to exist up to large masses [119]. A comparison between $\gamma\gamma \rightarrow t\bar{t}$ and $e^+e^- \rightarrow t\bar{t}$ should be interesting, since the two reactions couple to different charge conjugation eigenstates.

E. $\gamma\gamma$ Backgrounds in a PLC

Although the large $\gamma\gamma \rightarrow$ hadron cross section is a boon to QCD studies, it holds potential peril for the investigation of other physics. The time structure of bunch crossings in an S-band or X-band linear collider is such that individual bunches within a pulse-train cannot be resolved by the detector (typical spacings being 1-10 ns), so the effective luminosity per crossing is near 10^{31} cm^{-2} [44-46]. The total $\gamma\gamma \rightarrow$ hadron cross section is generally quoted at ~3×10^{-31} cm^2 (based on Vector Meson Dominance models) [6,8] leading to approximately three events per crossing. Fortunately, the overwhelming majority of these events are produced along the beamline at very low p_T (typically << 1 GeV) and so do not significantly affect the experimental environment [6,8].

It is possible, however, that the total $\gamma\gamma \rightarrow$ hadron cross section is much larger than 3×10^{-31} cm^2. Drees and Godbole have examined what they call 'once-resolved' and 'twice-resolved' photoproduction of hadrons in the context of studying potentially serious backgrounds at e^+e^- linear colliders [110,120]. In a once-resolved process a gluon or parton is 'pulled' out of the photon, leaving a low-p_T 'spectator jet,' and collides with another photon to produce two moderately high-p_T (a few GeV) 'mini-jets.' In a twice-resolved process a gluon or parton is pulled out of each photon, leaving two low-p_T spectator jets; the gluons or partons then fuse to form two mini-jets. The result is then two high-p_T mini-jets and one or two low-p_T spectator jets. Using the Drees–Grassie [121] parameterization of the gluon-parton densities in the photon, Drees and Godbole estimate the total $\gamma\gamma$ cross section to be near 2×10^{-30} cm^2, leading to approximately 20 events per crossing, with typically a few GeV of transverse energy per event [120]. Such a background obviously hinders a PLC's abilities as a physics tool. It should be noted, however, that the total cross section depends sensitively on the gluonic and partonic content of the photon at low Feynman x, quantities entirely unknown at present. It will take results from HERA to help determine how serious these backgrounds will be at a PLC.

The importance of such backgrounds could be drastically reduced, of course, if the luminosity per crossing could be reduced without sacrificing total luminosity. One such way to do this would be to discriminate between individual bunches in a pulse-train. Although it is unreasonable to expect this when using an X–band or S–band collider, superconducting accelerating structures allow this to be done naturally. The time structure of the electron bunches in a superconducting

linac is very different from that in a more conventional design; the TESLA collaboration proposes 400 bunches per pulse-train (at 20 pulse-trains/sec) with a spacing of 2 μs between bunches [48]. Detectors can easily distinguish between pulses so far apart, so in such a machine the luminosity per crossing is close to 2×10^{29} cm^{-2}. The Drees–Godbole $\gamma\gamma \rightarrow$ hadron cross section of 2×10^{-30} cm^2 then leads to only one event every two or three crossings. An additional advantage of a superconducting linac is that the low repetition rate (20 pulse-trains/sec) is much more closely matched to the present capabilities of high-power lasers.

IV. SUMMARY

The next e^+e^- machine built will surely be a high-luminosity (~$10^{33\text{-}34}$ cm^{-2} sec^{-1}), moderate energy ($\sqrt{s} \approx$ 300–500 GeV) linear collider. While such a collider will produce considerable physics in its own right, a significant enhancement of the physics program could be achieved by giving it the ability to produce and collide high energy photon beams. Indeed, physics at the time such an accelerator can be built may compel choosing the photon option over e^+e^- collisions. High power lasers with the right characteristics will soon exist which, via Compton backscattering off the linac electrons, will allow the generation of high energy photon beams with spot sizes similar to those possessed by the original electron beams. Furthermore, the luminosity of high energy $e\gamma$ and $\gamma\gamma$ collisions can exceed the potential e^+e^- luminosity, which is limited by the beamstrahlung effects due to high charge densities.

However, providing for photon collisions does impose restrictions on the accelerator, lasers, and detectors used in such a scheme. On the accelerator side, round or moderately elliptical beams are preferred, with beam sizes of order 50 nm at the interaction point. Bunch currents should be as high as possible in the linac, with bunch lengths reasonably small (~200 μm). Polarization of the electron beams (positrons not being required) will be a vital component of this facility. The conversion of the electron beams to photon beams must occur within a few centimeters of the interaction point to preserve the luminosity. The required laser(s) must have large energies (~10 J), short pulses (~3 ps), a large repetition rate (~100 Hz), diffraction-limited beams, and wavelengths in the near-infrared region (~1 μm) for use with colliders of energy 300 to 500 GeV. Difficult problems of engineering will include coupling the laser light into the interaction region, and the requirement of optical resonators to match the bunch trains in the accelerator. Also, the need to sweep the degraded electrons away from the interaction point will likely require a transverse magnetic field at the origin. Finally, although we have used the SLD detector for our simulations, a larger, more hermetic, finer-grained detector would be a better match to the physics we have considered.

A Photon Linear Collider capable of high energy $e\gamma$ and $\gamma\gamma$ collisions provides a unique opportunity for particle physics. A $\gamma\gamma$ collider serves as a tool to search for a Higgs boson in the

intermediate mass range, and to study a Higgs boson once found. With linac electron and laser polarization parameters chosen to provide a broad luminosity distribution, a $\gamma\gamma$ collider allows for the search for an intermediate mass Higgs boson in $\gamma\gamma \rightarrow b\bar{b}$ production. In such a scheme, the resulting high degree of mean photon helicity allows a significant reduction of the continuum $b\bar{b}$ background and an enhancement of the resonant Higgs signal. Additionally, as the Z boson does not couple to two photons, a $\gamma\gamma$ production scheme allows a search for a Higgs degenerate with the Z. Once found, study of the Higgs boson is possible with such a machine. With polarization parameters chosen to provide a more monochromatic spectrum, a $\gamma\gamma$ collider allows a measurement of the two-photon width of the Higgs, providing an opportunity to discriminate amongst various competing models of spontaneous symmetry breaking.

A PLC also offers the opportunity to search for new particles. Excited electron states can appear as resonances in $e\gamma$ scattering. Clean channels for the discovery of supersymmetric particles are available, primarily through single selectron production in association with a neutralino in $e\gamma$ collisions. Additionally, any particle with an appreciable two-photon coupling and pairs of heavy charged particles are accessible at such a machine.

Precision electroweak tests also benefit from a PLC. Photons in the initial state allow a test of the three-gauge boson coupling without the complicating effect of γ–Z interference. Both the $e\gamma \rightarrow W\nu$ and the $\gamma\gamma \rightarrow WW$ interactions offer information on the magnetic dipole moment and electric quadrupole moment of the W complementary to that available from $e^+e^- \rightarrow WW$. The $e\gamma \rightarrow eZ$ process permits a search for anomalous $\gamma\gamma Z$ and γZZ couplings.

Finally, a PLC allows an extension of the important Quantum Chromodynamics studies—begun at e^+e^- storage rings—to much higher energies. Studies of photon structure functions, jet and inclusive hadron production, exclusive hadron production, and $b\bar{b}$ and $t\bar{t}$ resonances are all made available at such a facility.

ACKNOWLEDGEMENTS

We would like to acknowledge valuable discussions with Tim Barklow, Mike Hildreth, Valery Khoze, Michael Perry, Valery Telnov, and Eran Yehudai.

REFERENCES

[1] R. H. Milburn, Phys. Rev. Lett. **10**, 75 (1963).

[2] I. F. Ginzburg et al., Pis'ma Zh. Eksp. Teor. Fiz. **34**, 514 (1981) [JETP Lett. **34**, 491 (1982)].

[3] C. Akerlof, SLC Workshop Notes, CN–39 (1981).

[4] J. E. Spencer, SLAC–PUB–2677 (1981).

[5] I. F. Ginzburg et al., Yad. Fiz. **38**, 372 (1983) [Sov. J. Nucl. Phys. **38**, 222 (1983)].

[6] I. F. Ginzburg et al., Nucl. Inst. Meth. **205**, 47 (1983); I. F. Ginzburg et al., Nucl. Inst. Meth. **219**, 5 (1984).

[7] J. C. Sens, preprint CERN–EP–88–99 (1988), in Proceedings of the VIIIth International Workshop on Photon–Photon Collisions, Jerusalem Hills, Israel, 1988, edited by U. Karshon (World Scientific, 1988).

[8] V. I. Telnov, Nucl. Inst. Meth. **A294**, 72 (1990).

[9] F. M. Renard, Z. Phys. **C14**, 209 (1982).

[10] I. F. Ginzburg et al., Nucl. Phys. **B228**, 285 (1983).

[11] K. O. Mikaelian, Phys. Rev. **D30**, 1115 (1984).

[12] A. Grau and J. A. Grifols, Nucl. Phys. **B233**, 375 (1984).

[13] G. Couture et al., Phys. Rev. **D39**, 3239 (1989).

[14] E. Yehudai, Phys. Rev. **D41**, 33 (1990).

[15] E. Yehudai, Phys. Rev. **D44**, 3434 (1991).

[16] S. Y. Choi and F. Schrempp, Phys. Lett. **B272**, 149 (1991).

[17] J. F. Gunion and H. E. Haber, preprint SCIPP–90/22 and UCD–90–25 (1990); presented at the 1990 DPF Summer Study on High Energy Physics, Snowmass, July 1990.

[18] T. Barklow, preprint SLAC–PUB–5364 (1990); presented at the1990 DPF Summer Study on High Energy Physics, Snowmass, July 1990.

[19] G. L. Kane, preprint UM–TH–91–02 (1991).

[20] M. Glück, Phys. Lett. **B129**, 255 (1983).

[21] J. A. Grifols and R. Pascual, Phys. Lett. **B135**, 319 (1984).

[22] J. A. Grifols and R. Pascual, Z. Phys. **C26**, 265 (1984).

[23] L. Bento and A. Mourao, Z. Phys. **C37**, 587 (1988).

[24] E. Reya, Phys. Lett. **B124**, 424 (1983).

[25] A. Goto and T. Kon, Europhys. Lett. **13**, 211 (1990); erratum Europhys. Lett. **14**, 281 (1991).

[26] H. P. Nilles, Phys. Rep. **110**, 1 (1984)

[27] H. E. Haber and G. L. Kane, Phys. Rep. **117**, 75 (1985).

[28] DELPHI Collaboration (P. Abreu et al.), Phys. Lett. **B245**, 276 (1990); ALEPH Collaboration (D. Decamp et al.), Phys. Lett. **B246**, 306 (1990); L3 Collaboration (B. Adeva et al.), Phys. Lett. **B248**, 203 (1990); OPAL Collaboration (M. Z. Akrawy et al.), Phys. Lett. **B253**, 511 (1991).

[29] J. F. Gunion et al., The Higgs Hunters Guide, Frontiers in Physics Series (Vol. 80), Redwood City, California (Addison Wesley, 1990).

[30] J. F. Gunion, preprint UCD–91–9 (1991).

[31] L. J. Hall and L. Randall, Phys. Rev. Lett. **65**, 2939 (1990).

[32] Particle Data Group (J. J. Hernandez et al.), Phys. Lett. **B239** (1990).

[33] S. Dawson et al., Proceedings of the 1984 Summer Study of the Design and Utilization of the Superconducting Super Collider, Snowmass, Colorado, edited by R. Donaldson and J. G. Morfin (Fermilab, 1985) p. 263.

[34] C. Dionisi and M. Dittmar, in Proceedings of the Workshop on Physics at Future Colliders, La Thuile, Italy and Geneva, Switzerland, 1987, edited by J. H. Mulvey (CERN, 1987) p. 149.

[35] T. G. Rizzo, Phys. Rev. **D40**, 2803 (1989).

[36] R. R. Volkas and G. C. Joshi, Phys. Rep. **159**, 303 (1988).

[37] R. Kleiss and P. M. Zerwas, in Proceedings of the Workshop on Physics at Future Colliders, La Thuile, Italy and Geneva, Switzerland, 1987, edited by J. H. Mulvey (CERN, 1987) p. 277.

[38] E. Farhi and L. Susskind, Phys. Rept. **74**, 277 (1981).

[39] K. J. F. Gaemers and G. J. Gounaris, Z. Phys. **C1**, 259 (1979).

[40] N. Isgur, preprint UTPT–89–13 (1989), in Proceedings of the BNL Workshop on Glueballs, Hybrids and Exotic Hadrons, Upton, NY, 1988, edited by Suh-urk Chung (AIP, 1988) p. 3.

[41] S. J. Brodsky and G. P. Lepage, preprint SLAC–PUB–4947 (1989), in Perturbative Quantum Chromodynamics, Advanced Series on Directions in High Energy Physics, Vol. 5, Teaneck, New Jersey, edited by A. H. Mueller (World Scientific, 1989) p. 93.

[42] Proceedings of the VIIIth International Workshop on Photon-Photon Collisions, Jerusalem Hills, Israel, 1988, edited by U. Karshon (World Scientific, 1988).

[43] M. Breidenbach et al., preprint SLAC–SLC–1991 (1990).

[44] Proceedings of the International Workshop on Next–Generation Linear Colliders, Stanford, California, edited by M. Riordan (SLAC, 1988), preprint SLAC–335 (1988).

[45] R. Ruth, preprint SLAC–PUB–5406 (1991).

[46] S. Iwata, preprint KEK–91–9 (1991).

[47] T. Weiland, to appear in the Proceedings of the 1991 Conference on Physics at Linear Colliders, Saariselka, Finland.

[48] Proceedings of the First International TESLA Workshop, Ithaca, New York, edited by H. Padamsee (Cornell, 1990) preprint CLNS–90–1029 (1990).

[49] For a review of linear collider prospects, see R. B. Palmer, Ann. Rev. Nucl. Part. Sci. **40**, 529 (1990).

[50] M. A. Johnson, M. D. Perry, and K. van Bibber, LLNL Internal Proposal (1991).

[51] V. M. Budnev et al., Phys. Rep. **15C**, 181 (1975).

[52] R. Blankenbecler and S. Drell, preprint SLAC–PUB–4810 (1988), in Proceedings of the 1988 Summer Study on High Energy Physics in the 1990's, Snowmass, Colorado, edited by S. Jensen (World Scientific, 1989) p. 683; R. Blankenbecler and S. Drell, Phys. Rev. Lett. **61**, 2324 (1988).

[53] D. V. Schroeder, SLAC–371 (1991), doctoral thesis (unpublished).

[54] I. F. Ginzburg et al., Yad. Fiz. **37**, 368 (1983) [Sov. J. Nucl. Phys. **37**, 222 (1983)]; I. F. Ginzburg et al., Yad. Fiz. **40**, 1495 (1984) [Sov. J. Nucl. Phys. **40**, 949 (1984)].

[55] V. E. Balakin and N. A. Solyak, preprint IYF–82–123 (1982); V. E. Balakin and N. A. Solyak, preprint SLAC–TRANS–0026 (1986), in Proceedings of 1986 Novosibirsk Conference on Particle Accelerators, v.1, Novosibirsk, USSR, edited by A. N. Skrinskii (Nauka, 1987), p. 151.

[56] V. I. Telnov and P. Chen, Phys. Rev. Lett. **63**, 1796 (1989).

[57] T. Maruyama et al., Phys. Rev. Lett. **66**, 2376 (1991).

[58] T. Nakanishi et al., preprint DPNU–91–23 (1991); T. Nakanishi et al., preprint KEK–91–51 (1991).

[59] Michael Perry, private communication.

[60] SLD Design Report SLAC–0273; M. Breidenbach, preprint SLAC–PUB–3798.

[61] M. Schneegans, preprint LAPP–EXP–91–04 (1991).

[62] Z. Kunszt et al., Phys. Lett. **B271**, 247 (1991).

[63] Mike Hildreth, private communication.

[64] Y. Okada et al., Prog. Theor. Phys. **85**, 1 (1991).

[65] H. E. Haber and R. Hempfling, Phys. Rev. Lett. **66**, 1815 (1991).

[66] J. Ellis et al., Phys. Lett. **B257**, 83 (1991).

[67] K. A. Isparin et al., Sov. J. Nucl. Phys. **11**, 712 (1970).

[68] T. Sjöstrand, Comp. Phys. Comm. **27**, 243 (1982); T. Sjöstrand, Comp. Phys. Comm. **39**, 3473 (1986); T. Sjöstrand and M. Bengtsson, Comp. Phys. Comm. **43**, 367 (1987).

[69] JADE Collaboration (W. Bartel et al.), Z. Phys. **C26**, 93 (1984).

[70] C. Baltay et al., in SLAC–354, Proceedings of the SLD Physics Week, Kirkwood, CA, 1989, p. 495.

[71] P. Mattig, Phys. Rept. **177**, 141 (1989).

[72] C. Bortoletto et al., Nucl. Inst. Meth. **A306**, 459 (1991).

[73] T. Aziz, Phys. Lett. **B265**, 445 (1991).

[74] L. F. Landau, Dok. Akad. Nauk USSR **60**, 207 (1948); C. N. Yang, Phys. Rev. **77**, 242 (1950).

[75] H. König, preprint OCIP–C–91–4 (1991).

[76] I. F. Ginzburg et al., preprint TF–28–182 (1990).

[77] K. Hagiwara et al., preprint DESY–91–107 (1991).

[78] E. Boos et al., preprint DESY–91–114 (1991).

[79] K. Kang and A. R. White, Phys. Rev. **D42**, 835 (1990).

[80] J. A. Grifols, Phys. Lett. **B264**, 149 (1991).

[81] F. M. Renard, preprint PM–91–17 (1991).

[82] F. M. Renard, Il Nuovo Cimento **A73**, 403 (1983).

[83] S. I. Polityko, Sov. J. Nucl. Phys. **43**, 93 (1986).

[84] S. J. Brodsky et al., Phys. Rev. Lett. **56**, 1763 (1986).

[85] M. Zahir, Phys. Rev. **D35**, 3338 (1987).

[86] N. S. Craigie et al., Fortschr. Phys. **34**, 261 (1986).

[87] H. Sazdjian, Phys. Lett. **B187**, 115 (1987).

[88] J. H. Kühn et al., Phys. Lett. **B158**, 270 (1985).

[89] A. Courau and P. Kessler, Phys. Rev. **D33**, 2024 (1983).

[90] I. F. Ginzburg and D. Yu. Ivanov, preprint TF–29–183 (1990).

[91] S. Komamiya, Phys. Rev. **D38**, 2158 (1988).

[92] K. Hagiwara et al., Nucl. Phys. **B282**, 253 (1987).

[93] G. L. Kane et al., Phys. Rev. **D39**, 2617 (1989).

[94] U. Baur, preprint MAD–PH–561 (1990).

[95] F. M. Renard, Nucl. Phys. **B196**, 93 (1982).

[96] Z. Ryzak, Nucl. Phys. **B289**, 301 (1989).

[97] S. J. Brodsky, Proceedings of the VIIIth International Workshop on Photon-Photon Collisions, Jerusalem Hills, Israel, 1988, edited by U. Karshon (World Scientific, 1988) p. 455.

[98] D. J. Miller et al., Proceedings of the ECFA Workshop on LEP 200, Aachen, Germany, 1986, edited by A. Bohm and W. Hoogland (CERN, 1987) p. 202.

[99] D. Bauer, Proceedings of the Workshop on Physics and Detector Issues for a High-Luminosity Asymmetric B Factory at SLAC, 1990, edited by D. Hitlin (SLAC, 1991) p. 173.

[100] R. S. Fletcher et al., Phys. Lett. **B266**, 183 (1991).

[101] H. C. Liu, Z. Phys. **C32**, 549 (1986).

[102] P. M. Zerwas, Proceedings of the VIIIth International Workshop on Photon-Photon Collisions, Jerusalem Hills, Israel, 1988, edited by U. Karshon (World Scientific, 1988) p. 380.

[103] J. H. Field, Proceedings of the VIIIth International Workshop on Photon-Photon Collisions, Jerusalem Hills, Israel, 1988, edited by U. Karshon (World Scientific, 1988) p. 349.

[104] A. Cordier and P. Zerwas, Proceedings of the ECFA Workshop on LEP 200, Aachen, Germany, 1986, edited by A. Bohm and W. Hoogland (CERN, 1987) p. 242.

[105] R. M. Godbole, preprint BU–TH–91–5 (1991).

[106] S. P. Li and H. C. Liu, Phys. Lett. **B143**, 489 (1984).

[107] M. Drees and R. M. Godbole, Phys. Lett. **B257**, 425 (1991).

[108] G. A. Ladinsky, Phys. Rev. **D39**, 2515 (1989).

[109] J. Layssac et al., Z. Phys. **C25**, 49 (1984).

[110] M. Drees and R. M. Godbole, Phys. Rev. Lett. **67**, 1189 (1991).

[111] See for example, S. J. Brodsky et al., Phys. Rev. **D19**, 1418 (1979).

[112] A. Nilsson, Proceedings of the VIIIth International Workshop on Photon-Photon Collisions, Jerusalem Hills, Israel, 1988, edited by U. Karshon (World Scientific, 1988) p. 261.

[113] See for example, M. Benayoun and V. L. Chernyak, Nucl. Phys. **B329**, 285 (1990); D. Morgan and M. R. Pennington, Z. Phys. **C48**, 623 (1990).

[114] S. J. Brodsky, preprint SLAC–PUB–5088 (1989).

[115] G. V. Jikia, preprint IFVE–91–33 (1991).

[116] F. Halzen et al., preprint MAD–PH–673 (1991).

[117] R. P. Kauffman, Phys. Rev. **D41**, 3343 (1990).

[118] P. M. Zerwas, preprint PITHA–90–32 (1990).

[119] H. Inazawa and T. Morii, Phys. Lett. **B247**, 107 (1990).

[120] M. Drees, to appear in the Proceedings of the 1991 Conference on Physics at Linear Colliders, Saariselka, Finland.

[121] M. Drees and K. Grassie, Z. Phys. **C28**, 451 (1985).